THE JOURNAL OF BIOLOGICAL CHEMISTRY VOL. 291, NO. 44, pp. 23343–23362, October 28, 2016
Published in the U.S.A.

Strategic Positioning and Biased Activity of the Mitochondrial Calcium Uniporter in Cardiac Muscle*[S]

Received for publication, August 26, 2016 Published, JBC Papers in Press, September 16, 2016, DOI 10.1074/jbc.M116.755496

Sergio De La Fuente[‡], Celia Fernandez-Sanz[§1], Caitlin Vail[‡1], Elorm J. Agra[‡], Kira Holmstrom[¶], Junhui Sun[‖], Jyotsna Mishra[§], Dewight Williams[**], Toren Finkel[¶], Elizabeth Murphy[‖], Suresh K. Joseph[‡], Shey-Shing Sheu[§], and György Csordás[‡2]

*From the [‡]MitoCare Center for Mitochondrial Imaging Research and Diagnostics, Department of Pathology, Anatomy, and Cell Biology, Thomas Jefferson University, Philadelphia, Pennsylvania 19107, the [¶]Center for Molecular Medicine, Laboratory of Molecular Biology, and the [‖]Systems Biology Center, Laboratory of Cardiac Physiology, NHLBI, National Institutes of Health, Bethesda, Maryland 20892, the [§]Center for Translational Medicine, Thomas Jefferson University, Philadelphia, Pennsylvania 19107, and the **Penn EM Resource Laboratory, University of Pennsylvania, Philadelphia, Pennsylvania 19104*

Control of myocardial energetics by Ca^{2+} signal propagation to the mitochondrial matrix includes local Ca^{2+} delivery from sarcoplasmic reticulum (SR) ryanodine receptors (RyR2) to the inner mitochondrial membrane (IMM) Ca^{2+} uniporter (mtCU). mtCU activity in cardiac mitochondria is relatively low, whereas the IMM surface is large, due to extensive cristae folding. Hence, stochastically distributed mtCU may not suffice to support local Ca^{2+} transfer. We hypothesized that mtCU concentrated at mitochondria-SR associations would promote the effective Ca^{2+} transfer. mtCU distribution was determined by tracking MCU and EMRE, the proteins essential for channel formation. Both proteins were enriched in the IMM-outer mitochondrial membrane (OMM) contact point submitochondrial fraction and, as super-resolution microscopy revealed, located more to the mitochondrial periphery (inner boundary membrane) than inside the cristae, indicating high accessibility to cytosol-derived Ca^{2+} inputs. Furthermore, MCU immunofluorescence distribution was biased toward the mitochondria-SR interface (RyR2), and this bias was promoted by Ca^{2+} signaling activity in intact cardiomyocytes. The SR fraction of heart homogenate contains mitochondria with extensive SR associations, and these mitochondria are highly enriched in EMRE. Size exclusion chromatography suggested for EMRE- and MCU-containing complexes a wide size range and also revealed MCU-containing complexes devoid of EMRE (thus disabled) in the mitochondrial but not the SR fraction. Functional measurements suggested more effective mtCU-mediated Ca^{2+} uptake activity by the mitochondria of the SR than of the mitochondrial fraction. Thus, mtCU "hot spots" can be formed at the cardiac muscle mitochondria-SR associations via localization and assembly bias, serving local Ca^{2+} signaling and the excitation-energetics coupling.

Mitochondrial Ca^{2+} uptake in response to cytosolic calcium signals has been emerging as a pivotal means for tuning oxidative ATP production to energy demands but also as risk factor for Ca^{2+} overload, oxidative stress, and ignition of cell death pathways. The inside negative membrane potential across the IMM[3] ($\Delta\Psi_m$) is a tremendous driving force for Ca^{2+} uptake that is implemented via the tightly regulated Ca^{2+}-activated Ca^{2+} channel, mtCU (1, 2). Recent research identified mtCU as a hetero-oligomeric complex of subunits, the "uniplex" (3). Of these subunits, the pore-forming MCU and the single-pass transmembrane protein EMRE have proven essential for functional channel formation in mammalian cells (4–7). MICU1 and -2 are Ca^{2+}-sensing EF-hand proteins in the intermembrane space that regulate Ca^{2+} gating of the channel, and MICU1 seems to be required for the association of MICU2 with the mtCU complex (uniplex) (see Ref. 8 for a review). MICU1 has been proposed to require EMRE to associate with the mtCU complex (3). In this regard, EMRE has been recently shown to interact with MCU via its transmembrane domain and with MICU1 via its C-terminal acidic tail in the intermembrane space. This would help to retain MICU1 with the MCU-EMRE complex; otherwise, MICU1 can bind to MCU without EMRE (5). The functionally dominant negative MCU homologue MCUb can directly hetero-oligomerize with MCU (9). Although tissue variations occur, optimal activation of mtCU to decode rapid signaling events usually requires cytosolic [Ca^{2+}] ([Ca^{2+}]$_c$) exposure that exceeds the global peak levels (10). Such exposure is established at focal associations with the SR in close proximity of activated Ca^{2+} release channels (RyR2 in the heart). The myocardial contractile cycle is predominantly

* This work was supported by NHLBI, National Institutes of Health, Grant RO1 HL122124 (to G. C. and S. S. S.), by American Heart Association Postdoctoral Fellowship 16POST27770032 (to S. F.), and National Institutes of Health Grant RO1 DK103558 (to S. K. J.). The authors declare that they have no conflicts of interest with the contents of this article. The content is solely the responsibility of the authors and does not necessarily represent the official views of the National Institutes of Health.

[S] This article contains supplemental Video S-1.

[1] Both authors contributed equally to this work.

[2] To whom correspondence should be addressed: MitoCare Center for Mitochondrial Imaging Research and Diagnostics, Dept. of Pathology, Anatomy, and Cell Biology, Thomas Jefferson University, Suite 527J Jefferson Alumni Hall, 1020 Locust St., Philadelphia, PA 19107. Tel.: 215-955-4556; Fax: 215-923-2218; E-mail: Gyorgy.Csordas@jefferson.edu.

[3] The abbreviations used are: IMM, inner mitochondrial membrane; mtCU, IMM Ca^{2+} uniporter; [Ca^{2+}]$_c$, cytosolic [Ca^{2+}]; [Ca^{2+}]$_m$, mitochondrial [Ca^{2+}]; SR, sarcoplasmic reticulum; jSR, junctional SR; OMM, outer mitochondrial membrane; VDAC, voltage-dependent anion channel; CSQ, calsequestrin; IF, immunofluorescence; BDM, 2,3-butanedione monoxime; TEM, transmission electron microscopy; AF, Alexa Fluor®; WB, Western blotting; MAM, mitochondria-associated reticular membrane; MAO, monoamine oxidase; SDH, succinate dehydrogenase; Tg, thapsigargin; CP, contact point.

fueled by mitochondrial oxidative metabolism and driven by RyR2-derived Ca^{2+} signals. Propagation of these signals to the mitochondria as a feed-forward metabolic tuning loop (excitation-energetic coupling) has long been established (11–14). It has been recently suggested that mitochondrial Ca^{2+} uptake during "baseline" pacing is very small; it does not shape $[Ca^{2+}]_c$ spikes but becomes significant upon stress (15). Germ line ablation of MCU in mice also suggested dispensability for baseline myocardial activity and even for stress tolerance (16, 17). In conditional, short term cardiac MCU KO, on the other hand, impairment of metabolic and contractile adaptation to adrenergic stress revealed the need for mitochondrial Ca^{2+} uptake in the adaptive response (18, 19). The above mentioned effects of short term cardiac MCU ablation were also phenocopied by cardiac muscle-specific transgenic expression of a dominant negative MCU (20).

With a large mitochondrial population perpetually being exposed to rapid $[Ca^{2+}]_c$ oscillations, precisely controlled mitochondrial delivery of Ca^{2+} signals is critical in the ventricular cardiomyocytes to support excitation-energetic coupling without Ca^{2+} overload. In line with a tighter Ca^{2+} uptake control, cardiac muscle mitoplasts presented the lowest mtCU activity (current density) among a range of different tissues (21). Because adult cardiac mitochondria are relatively large with greatly enhanced IMM surface by abundant cristae invaginations, the relatively scarce mtCU, if evenly distributed, would have little chance to effectively mediate local delivery of Ca^{2+} from RyR2-derived nanodomains. We have shown earlier that junctional SR (jSR or dyadic SR)-mitochondria associations align with IMM-OMM contact points (hereafter referred to as "contact points") and reasoned that this would shorten the path for Ca^{2+} from the RyR2 to the IMM (22). This implied that mtCU would be present at the contact points, with which mitochondria-jSR associations are aligned. With the molecular building blocks revealed (23), it is now testable whether location-specific variances in mtCU could contribute to effective Ca^{2+} signal reception by cardiac mitochondria. Here, via fractionation and immunovisualization approaches as well as Ca^{2+} uptake assays, we identify biases in the localization and subunit composition of the mtCU that lead to more effective Ca^{2+} uptake at the area of mitochondria-jSR associations.

Results

Distribution Bias of mtCU toward Contact Points—Mitochondria-jSR associations have been shown to form over contact point-containing mitochondrial surface segments (22). We speculated that SR-derived Ca^{2+} release would expose mtCU optimally if it was located at contact points and/or the inner boundary membrane as opposed to being deep inside the cristae. To this end, submitochondrial membrane fractions (Fig. 1*A*) enriched in OMM, contact points, and IMM were probed for the mtCU constituents MCU and EMRE. For reference, the OMM porin voltage-dependent anion channel (VDAC) was most abundant in the OMM-rich fraction (severalfold enrichment against the contact point-rich fraction; Fig. 1, *B* and *C*). The IMM protein mitofilin/Mic60, a constituent of cristae junctions (and contact points) showed similar enrichment in the contact point-rich fraction against the IMM-rich fraction but was practically absent from the OMM-rich fraction. The SR-resident calsequestrin (CSQ; marking mitochondria-associated jSR) was most (~2-fold) enriched in the contact point-rich fraction (Fig. 1, *B* and *C*). Importantly, MCU and EMRE both showed enrichment similar to that of CSQ and mitofilin/Mic60 in the contact point-rich fraction when compared with the IMM-rich fraction, consistently with a contact point-directed location bias. Finally, another IMM-resident prohibitin with no reported contact point preference was similarly abundant in contact point-rich and IMM-rich fractions while essentially missing from the OMM-rich fraction. To verify a preferred localization to the inner boundary membrane *in situ*, MCU immunofluorescence distribution was referenced to the matrix protein mtHsp70 in glass-mounted mitochondria (mitochondrial fraction) by means of 3D super-resolution/single-molecule microscopy (Fig. 2). mtHsp70 immunofluorescence was broadly almost completely overlapping with the matrix probe MtTrRed in isolated rat cardiomyocytes when visualized via confocal microscopy (Fig. 2*A*). In the glass-mounted mitochondrial fraction, the mtHsp70 immunofluorescent particles, imaged via 3D super-resolution microscopy, essentially "filled" the individual mitochondrial volumes (Fig. 2*B*). The much scarcer anti-MCU particles were ~2.5 times more prevalent at the periphery than inside the volume filled by mtHsp70 labeling (Fig. 2*B*, supplemental Video S-1), consistent with a distribution bias to the inner boundary membrane. Similar results could be obtained when MCU immunofluorescence was referenced to mtHsp70 in primary cardiomyocytes by means of a different super-resolution approach (see Fig. 4*D*). Taken together, the above results show that mtCU preferentially locates close to the cytosolic boundary of the mitochondrion (Figs. 1, 2, and 4*D*) at the contact points (Fig. 1) and so is highly accessible to Ca^{2+} derived from SR release when entering through the OMM.

Distribution Bias of MCU toward Mitochondria-jSR Associations in Isolated Cardiac Mitochondria—To correlate MCU distribution to mitochondria-jSR associations, its colocalization with RyR2 was evaluated using IF assays. Consistent with earlier published data (17), MCU protein was absent in the MCU KO cells as confirmed by Western blot (data not shown). The mitochondrial fraction is known to contain mitochondria-associated jSR fragments that occur in confocal images as discrete RyR2 immunofluorescent particles over the mitochondrial surface and that are capable of RyR2-dependent Ca^{2+} delivery to the mitochondrial matrix (24). First, we used this preparation for IF experiments to minimize cross-reactions that were apparent in primary cardiomyocytes when using the Sigma HPA016480 MCU antibody. For the MCU KO mitochondrial fraction, the IF labeling by this antibody was <10% of that in the control (Fig. 3*A*). Also, specific anti-MCU labeling for the mitochondrial fraction required permeabilization (not shown), confirming that the antibody had to cross organelle membrane(s) (OMM and IMM) to bind its epitope. Anti-MCU and anti-RyR2 IF colocalization was examined in the mitochondrial fraction of rat and mouse heart. The corresponding IF patterns counterlabeled with the mitochondrial matrix probe MtTrRed are shown in Fig. 3, *B* (rat) and *C* (mouse). Colocalization analysis of MCU with RyR2 is schematized in Fig. 3*D*,

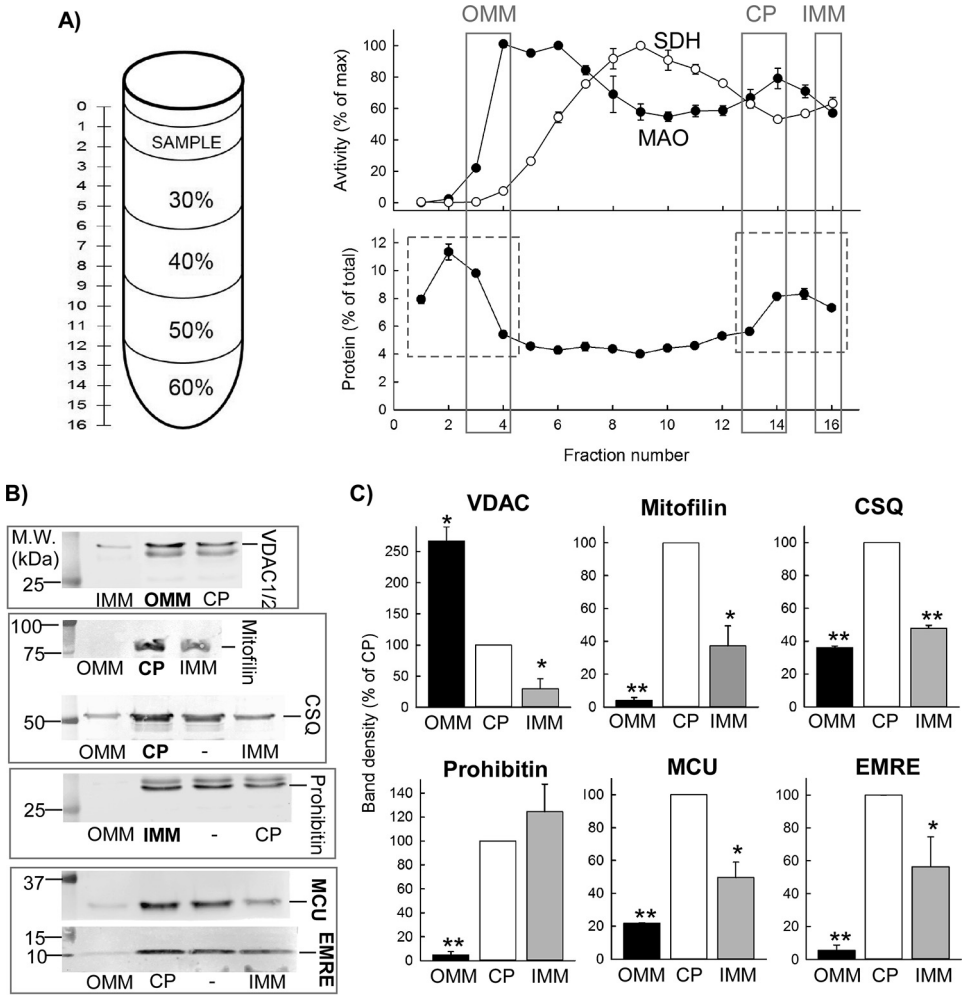

FIGURE 1. **MCU and EMRE are enriched in the mitochondrial contact points.** *A*, submitochondrial membrane fractions obtained via osmotic and ultrasonic rupture of mitochondria from rat heart homogenates were separated on a 30–60% quasicontinuous sucrose gradient (layered as shown with fraction numbers aligned on the *left*). On the *right*, enzyme profiles (*top*) of the OMM-resident MAO and the IMM-bound SDH along with the protein profile (*bottom*) of the submitochondrial fractions are shown. Fractions from the two protein peaks richest in OMM (*OMM*, first MAO peak before SDH increase), contact points (*CP*, second MAO peak at high SDH), and IMM (*IMM*, MAO minimum after its second peak) are labeled accordingly and selected by *gray rectangles*. *B*, representative WB of the indicated mitochondrial and SR proteins in the indicated submitochondrial fractions. Some of the blots also contain non-relevant lanes (sample prepared/treated differently) that are *labeled* with a *hyphen*. *C*, relative abundances (normalized to CP) of OMM proteins (the voltage-dependent anion channels VDAC1/2), IMM proteins (mitofilin/Mic60, MCU, EMRE, prohibitin), and SR-resident proteins (calsequestrin, CSQ). Note the enrichment of mitofilin/Mic60, MCU, EMRE, and CSQ but not prohibitin in the CP ($n = 3$ rats, for the enzyme assays 3 technical replicates each). *Error bars*, S.E. *, $p \leq 0.05$; **, $p \leq 0.01$.

depicting a mitochondrion associated with a jSR and two MCUs located at or away from the jSR interface (*top*). The association with jSR is mostly confined to the transversal side (one or both). In the *middle*, a mitochondrion is represented by a *cylinder* with *equal height* and *diameter* (not elongated). For such a shape one transversal side would represent ~17% (one-sixth) of the total surface, which is also the portion of MCU that would locate there if evenly distributed. This percentage would be even lower for an elongated cylinder that would correspond to the majority of intermyofibrillar mitochondria. The *colored discs* at the *bottom* illustrate the fluorescence signals emitted by the IF fluorophores or MtTrRed with consideration of the ~250–330 nm diffraction limit in resolution. After binarization (thresholding), anti-MCU and anti-RyR2 immunofluorescent spots with overlap (crossing, *x*) were accounted as colocalized (MCU_x and RyR_x; non-colocalized are •MCU and •RyR). The percentage overlap between MCU and RyR2 IF spot areas (*yellow segment*) was ~12–13%, consistent with the two molecules residing in different compartments. Notably, most RyR2 spots did display overlap with MtTrRed (regardless of colocalization with MCU), suggesting that they resided in mitochondria-associated jSR. MCU and RyR2 IF spot counts per field (of ~1,300 μm^2) were 30.5 ± 2 and 57 ± 3.6, respectively, in the rat, whereas they were 42.5 ± 3.5 and 134 ± 7 in the mouse. Importantly, the percentage of MCU IF spots colocalizing with RyR2 spots was 50 ± 4.5% for the rat and 56 ± 3% for the mouse (Fig. 3*E*). Thus, over half of the distinct MCU-positive structures had overlap with RyR2 labeling, which is more than what would be expected upon even distribution. Of note, in murine cardiac muscle, not all mitochondria have close contact with dyads, and some of the anti-MCU IF spots that did not colocalize with RyR2 must have derived from those mitochondria.

Distribution Bias of MCU toward Mitochondria-jSR Associations in Primary Adult Cardiomyocytes—To further establish MCU distribution in the cardiac muscle mitochondria *in situ* in the context of the myocyte architecture, colocalization of MCU

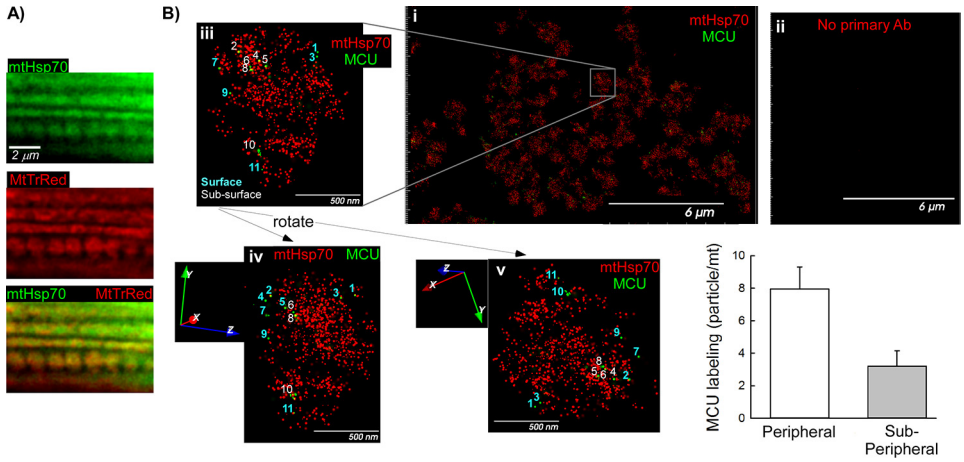

FIGURE 2. **MCU distribution and clusterization in glass-mounted mitochondria resolved by 3D super-resolution microscopy.** Anti-MCU IF distribution was correlated with that of the matrix marker mtHsp70 in coverglass-mounted mitochondrial fraction isolated from rat heart. Super-resolution imaging was carried out as described under "Experimental Procedures." *A*, reference confocal images showing closely overlapping mtHsp70 IF (*green*) and (matrix-loaded) MtTrRed fluorescence (*red*) in a primary cardiomyocyte. *B*, low magnification overview (*i*) of a group of mitochondria defined by discrete 3D (no rotation, *z* axis is perpendicular to the image plane) clouds of mtHsp70 immunofluorescent particles (Alexa 647-conjugated antibodies). *ii*, IF control without primary antibody. The mitochondrion in the *gray rectangle* (*i*) is *enlarged* (*iii*) and shown in two additional rotation angles (*iv* and *v*; see the *red-green-blue x-y-z arrows* for orientation) to reveal the position of the anti-MCU labeling (*green dots* representing Cy3b-conjugated secondary antibodies) in the volume filled by the mtHsp70. In the different rotational views, the *numbers* label MCU-positive "peripheral" particles that in the given plane could be moved away without having to pass/cross mtHsp70 particles (*cyan numbers*) and "subperipheral or internal" particles that are deeper in the mtHsp70 point cloud (*white numbers*). Note that in the different rotational views peripheral particles may appear inside the *red point cloud* when they are positioned in front or behind the cloud (*e.g.* particles 2 and 4 in *rotation panel iii* look subperipheral (*white*), whereas in *rotation panel iv*, they turn out to be peripheral (*cyan*)). An anti-MCU particle was classified as "peripheral" if in any rotation plane it was found to be peripheral. The bar chart summarizes these evaluations ($n = 1$ rat). *Error bars*, S.E.

and RyR2 IF in freshly isolated primary adult cardiomyocytes was investigated. To better resolve the constellation of the proteins, two super-resolution approaches were employed. The primary anti-MCU antibody had to be changed from the Sigma HPA016480 to the Cell Signaling Technologies D2Z3B because the former displayed too much nonspecific labeling in the MCU KO myocytes (Fig. 4*A*, *i–iv versus v–x*). First, using the same fluorophores as for the isolated mitochondria (Fig. 3), the IF distributions were imaged using the Airyscan detector of the Zeiss LSM880 confocal system. This technology allows us to go $\times\sim$1.7 beyond the diffraction limit in an otherwise conventional laser-scanning confocal setup. Fig. 4*B* shows the overview of MCU and RyR2 IF distribution over a myocyte (*iii–v*). The *enlarged area* (*vi*) reveals numerous MCU particles (*red*) in close vicinity of RyR2 (*green*). For reference, MCU IF was also examined in the context of the matrix protein mtHsp70 (Fig. 4, *B* (*vii–x*) and *D*). Due to the higher resolution, colocalization was evaluated based on proximity and not on actual overlapping fluorescence pixels; the binarized RyR2 fluorescence masks were expanded radially by 66 nm (1 pixel), and the MCU masks overlapping with the expanded RyR2 mask were counted (Fig. 4*C*). As the bar graph in Fig. 4*C* shows, 45.7 ± 1.3% of the MCU spots were in the close vicinity of RyR2, whereas >85% colocalized with mtHsp70. MCU IF was also referenced to the outlines of clearly distinguishable intermyofibrillar mitochondria defined by the mtHsp70 fluorescence. Here, over individual mitochondrial (mtHsp70) areas, MCU immunofluorescent particles were grouped by whether or not they were in contact with the boundary line (peripheral) and also by how many peripheral MCUs were located on transversal and longitudinal sides (Fig. 4*D*). Consistent with a location preference toward the inner boundary membrane/contact points, ~85% of the MCU particles were peripheral (Fig. 4*E*). Importantly, 52 ± 4% of the MCU IF particles were in contact with transversal sides (where dyad association can occur), whereas only 33 ± 4% were in contact with longitudinal sides despite their elongated shape (Fig. 4*E*, *T versus L*).

Finally, MCU and RyR2 IF distribution were also evaluated via true nanoscopy using the Vutara350 single-molecule imaging system. Fig. 5*A* shows example images of the point cloud representation of the secondary antibody-conjugated fluorophores CF™ 568 (RyR2; *green*) and Alexa Fluor® (AF) 647 (MCU; *red*) without further image filtering (*i* and *ii*) and after applying a 5 × 5-pixel Gaussian blur (*iii* and *iv*). Colocalization of MCU and RyR2 was evaluated via nearest neighbor distance analysis in the non-filtered point cloud. >55% of the MCU-bound antibodies had an RyR2-bound neighbor in ≤150-nm distance, and ~40% had a neighbor in ≤100-nm distance (Fig. 5*B*, *top bar chart*), numbers that are quite consistent with the colocalization data obtained by the confocal and Airyscan approaches. For reference, ~95% of the MCU-bound antibodies had an mtHSP70-bound neighbor in ≤100-nm distance and 100% in ≤150-nm distance (Fig. 5*B*, *bottom bar chart*). Collectively, these colocalization data obtained from primary adult cardiomyocytes further reinforced an MCU distribution bias toward mitochondria-dyad associations, consistent with the idea of mtCU hot spots in these areas.

MCU Localization to the Dyads Is Promoted by Ca^{2+} Signaling Activity—As for what would drive the above established MCU distribution bias toward the dyad areas, one obvious candidate was the Ca^{2+} signaling activity attributed to the dyads. To this end, the colocalization of MCU and RyR2 IF was (re)evaluated in freshly isolated adult ventricular myocytes that were superfused either by Ca^{2+}-containing ($[Ca^{2+}]_e \sim 1$ mM) or in quasi-Ca^{2+}-free ($[Ca^{2+}]_e \sim 2$ μM, just enough to prevent detachment) incubation buffer under 2-Hz electric field stimu-

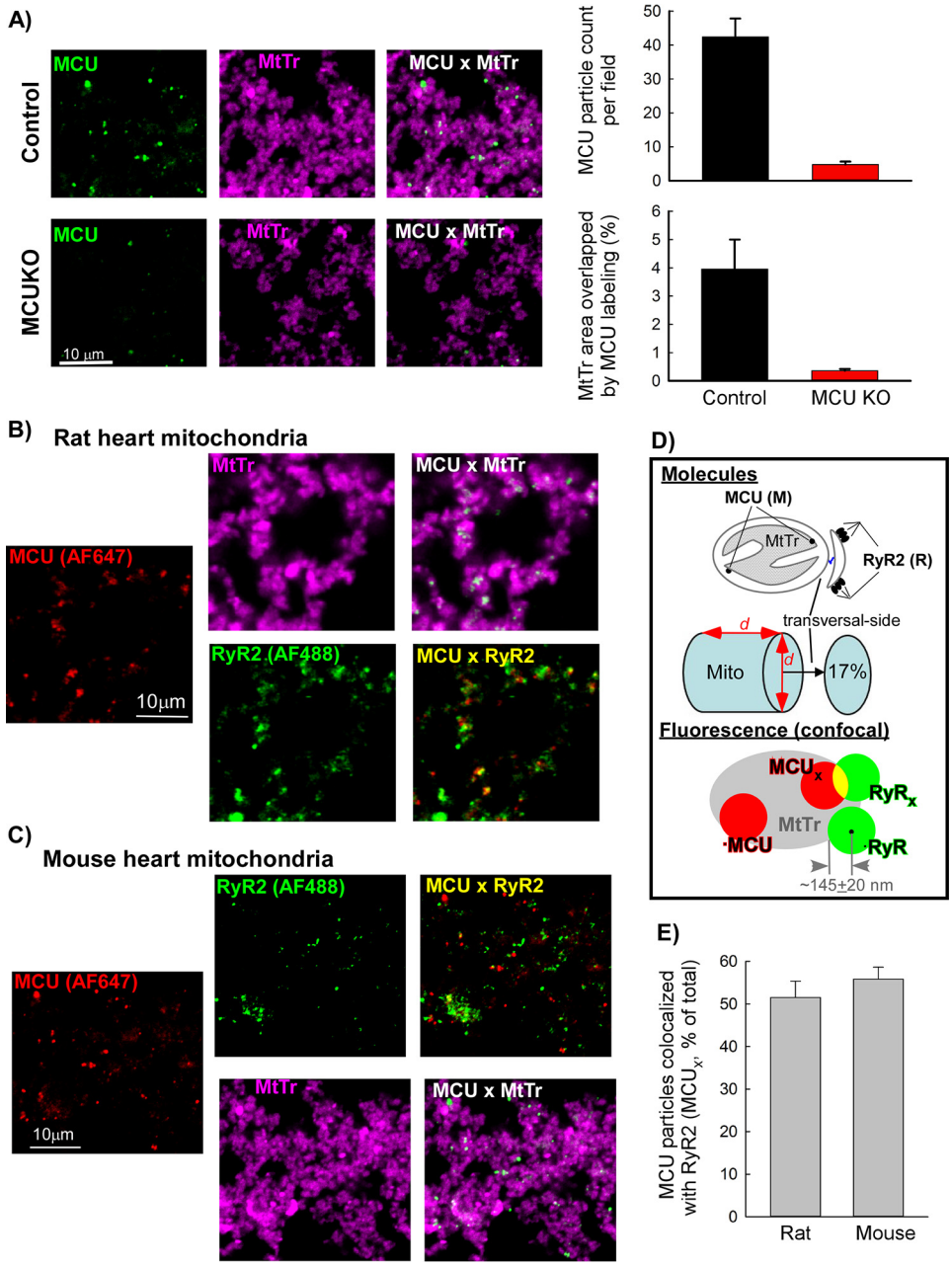

FIGURE 3. **Validation of MCU IF and colocalization between MCU and RyR2 in cardiac mitochondrial fractions.** Shown is the distribution of anti-MCU IF (AF 647; *red*), anti-RyR2 (AF 488; *green*), and the mitochondrial matrix probe MtTrRed (*MtTr*) fluorescence (*purple*) in mouse and rat cardiac mitochondrial fractions. The mitochondria are shown in the images separately and/or overlaid. *A*, mitochondrial fraction isolated from control (*top*) and MCU KO (*bottom*) mouse hearts, glued to coverslips, and loaded with MtTrRed. Bar charts show the number of MCU IF-positive particles per field (*top*) and the mitochondrial area (percentage of MtTrRed staining) covered by MCU IF labeling (*bottom*). Note the >90% reduction in anti-MCU labeling in the MCU KO. *B* and *C*, anti-MCU and anti-RyR2 IF labeling of coverglass-mounted membrane particles from the mitochondrial fraction of rat (*B*) and mouse (*C*) heart. The images show anti-MCU IF in *red*, anti-RyR2 IF in *red*, and MtTrRed fluorescence in *purple*. The *gray frames* enclose different fluorescence images from the same field. *D*, the scheme explains the colocalization analysis. See "Results" for details. *E*, percentage amount of MCU particles colocalizing with RyR2 in the rat and mouse. $n = 3$ control mice, 2 MCU KO mice, and 3 rats; technical replicates, 5 fields each. *Error bars*, S.E.

lation before fixation. Contractile activity was suspended pharmacologically (2,3-butanedione monoxime (BDM)). As Fig. 6*A* shows, there was no significant difference in the RyR2 IF pattern and metrics (sarcoplasm area occupied was 8.7 ± 0.2 *versus* 8.6 ± 0.7%) at the different $[Ca^{2+}]_e$ levels. The size of MCU IF particles did not change either (mean Feret's diameter was 0.33 μm for both). However, the extracellular Ca^{2+} removal that eliminated the pacing-associated $[Ca^{2+}]_c$ oscillations (Fig. 6*B*) also significantly decreased the percentage of MCU particles in close vicinity of RyR2 (Fig. 6*C*). These data thus strongly suggest that Ca^{2+} signaling activity is one of the driving mechanisms that recruit MCU to the jSR interface areas.

The SR Fraction Contains Mitochondria with Extensive Reticular Associations and with a Distinct Protein Profile with High Levels of EMRE—The tissue homogenates, from which mitochondrial and SR fractions were isolated, had been prepared without enzymatic digestion to preserve SR-mitochondrial tethers. We postulated that although the SR fraction contained

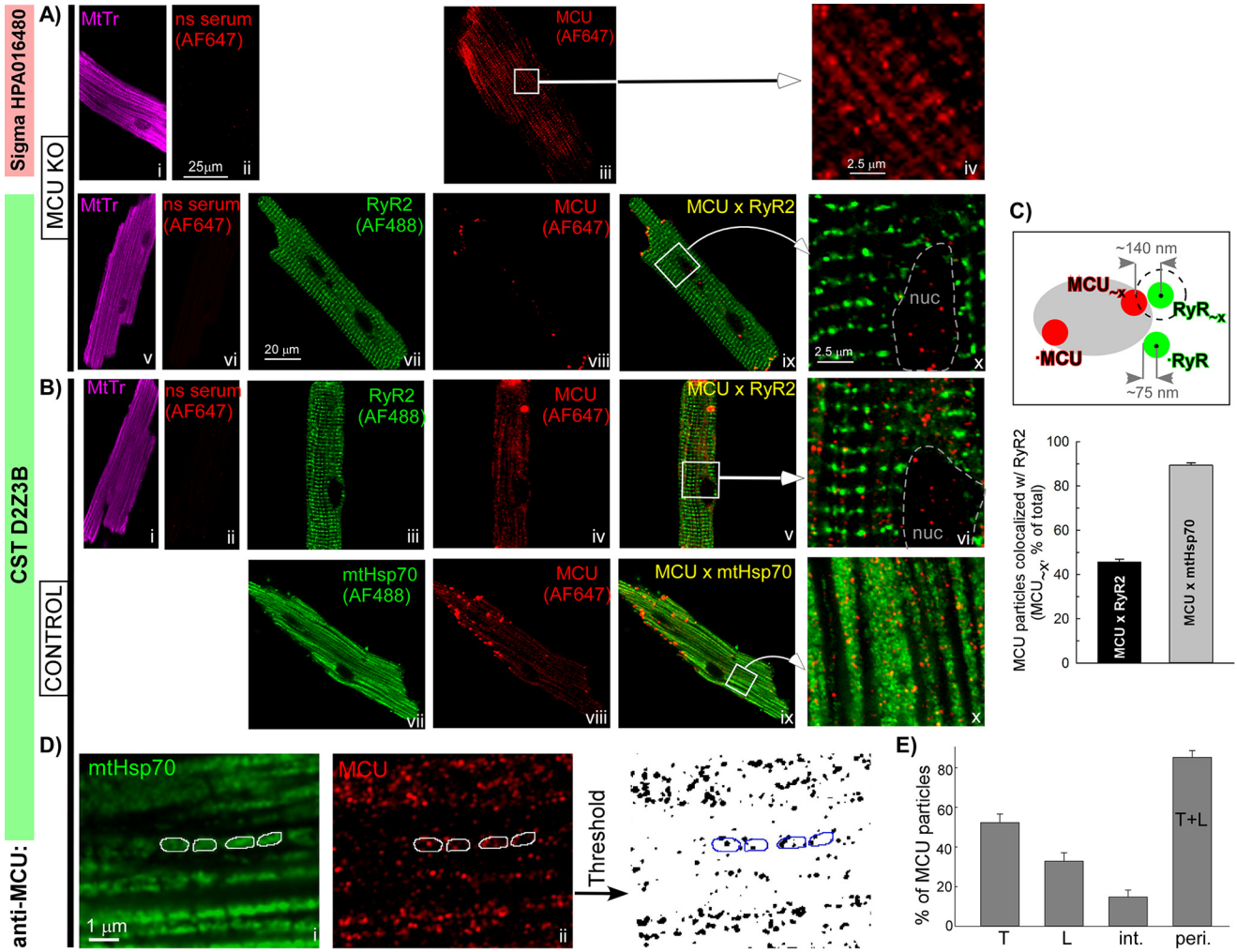

FIGURE 4. **MCU IF distribution in the context of RyR2 and mitochondrial shape (mtHsp70) in adult mouse cardiomyocites visualized by the Zeiss LSM880 Airyscan super-resolution system.** *A*, validation of two anti-MCU antibodies (Sigma and Cell Signaling as labeled on the *left*) for IF in primary adult mouse cardiomyocytes lacking MCU (*MCU KO*). MtTrRed (*MtTr*) distribution and negative control (nonspecific (*ns*) serum in place of primary antibody) overview images of representative myocytes are shown in *i*, *ii*, *v*, and *vi*. *iii* and *iv*, an overview of the Sigma antibody distribution over a myocyte and a ×8 zoom of the indicated area, respectively. Note the extensive IF labeling throughout the cell. *vii* and *viii*, overviews of RyR2 (*green*; AF 488) and the Cell Signaling MCU antibody (*red*; AF 647) IF distribution over a myocyte separately and then overlaid in *ix* and enlarged (×8) from the indicated area in *x*. Note that the bulk of the sarcoplasmic area is clear of MCU IF (also compare with *B*, *iv–vi*) with the exemption of the nuclear areas (*nuc*) and some aggregates mostly at the cell edges. *B*, IF co-labeling of MCU (Cell Signaling) with RyR2 (*iii–vi*) and MCU with mtHsp70 (*vii–x*) in control cardiomyocytes. *i* and *ii*, show MtTrRed distribution and negative IF control, respectively. *iii* and *iv*, overviews of RyR2 and MCU IF distribution over a myocyte separately and then overlaid in *v*, and enlarged (×8) in *vi*. Following the same order of image arrangement, mtHsp70 and MCU IF distributions in a myocyte are shown in *vii–x*. *C*, colocalization analysis of MCU × RyR2 and MCU × mtHsp70 IF. Due to the higher resolution, colocalization was determined by proximity and not actual IF overlap as depicted in the scheme and explained further under "Results." The ~75-nm radius for RyR fluorophore (~520-nm emission → ~260-nm diffraction limit for particle diameter) is calculated by dividing the estimated diffraction-limited value by 1.7. The bar chart shows the percentage of MCU IF particles at ≤66-nm distance from the edge of RyR2 (*black bar*) and mtHsp70 particles (*gray bar*). *D*, MCU distribution analysis over individual mitochondria. MCU IF particle distribution was referenced to masks drawn over individual mitochondria (mtHsp70 IF). Thresholded MCU particles over each mask were classified according to whether or not they contacted the contour (peripheral (*peri.*) *versus* internal (*int.*)) and whether they contacted the transversal (*T*) or longitudinal (*L*) contour side. The bar chart in *E* summarizes the analysis. $n = 4$ control mice, 2 MCU KO mice; technical replicates, 10 cells each. *Error bars*, S.E.

a smaller portion of mitochondrial membranes than the mitochondrial fraction, this smaller portion would be composed of mitochondria with a larger surface segment interfacing with jSR. Indeed, transmission electron micrographs of high pressure frozen suspensions of rat heart mitochondrial fraction (Fig. 7*A*), when compared with those of the SR fraction (Fig. 7*B*), contained more numerous (~5 times; Fig. 7*D*) and larger (0.19 ± 0.05 μm^2 *versus* 0.43 ± 0.03 μm^2; Fig. 7*C*) mitochondria. However, a larger portion of the mitochondrial cross-sections displayed associations with membrane vesicles in the SR fraction than in the mitochondrial fraction (Fig. 7*E*, *top*). Also, for vesicle-associated mitochondria, the number of vesicles per mitochondrion and even more per the mitochondrial perimeter length was substantially larger in the SR than in the mitochondrial fraction (Fig. 7*E*).

Glass-attached MtTrRed-loaded mitochondria of the SR fraction had more RyR2 IF-labeled particles than those of the mitochondrial fraction; however, the number of RyR2 particles per area unit of the MtTr labeling was disproportionally larger, consistently with more extensive mitochondrial-jSR associations (Fig. 8*A*).

If the mtCU complex was concentrated to mitochondria-jSR associations, its constituents would probably be more represented among the mitochondrial proteins of the SR than the

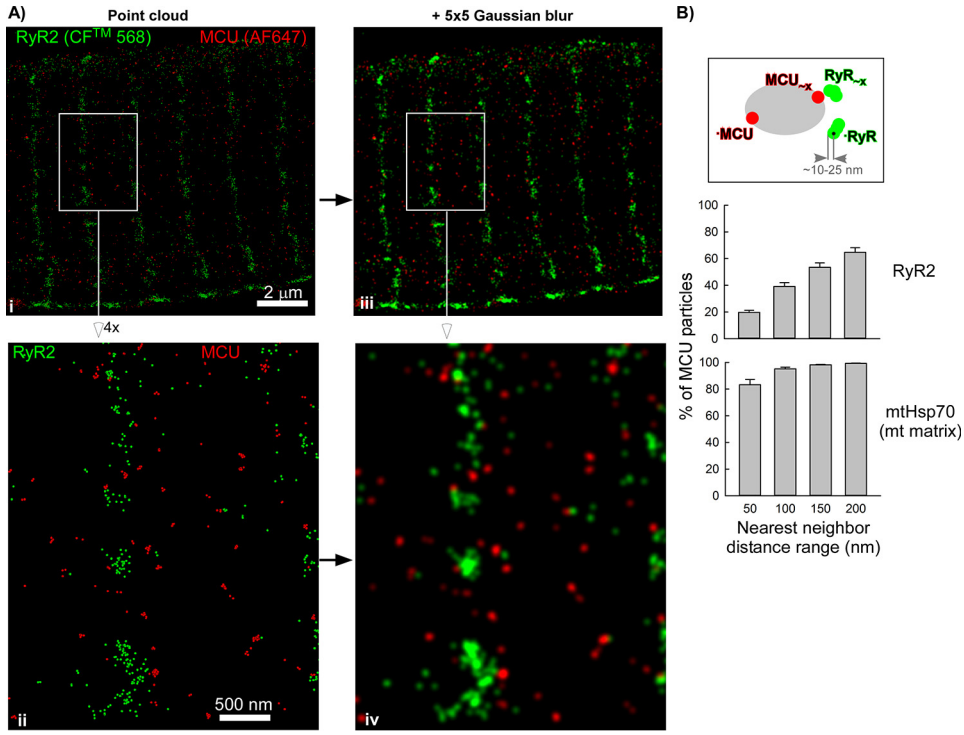

FIGURE 5. **MCU and RyR2 IF colocalization resolved by the Vutara 350 single-molecule super-resolution microscopy in adult cardiomyocytes.** *A*, mouse adult cardiomyocites were labeled with anti-MCU (AF 647; *red*) and anti-RyR2 (CF™ 568; *red*). The *left panels* show point cloud images (*i* and *ii*), and the *right panels* show a 5 × 5 Gaussian blur filtering (*iii* and *iv*). *ii* and *iv*, ×4 enlargements of the indicated areas from *i* and *ii*, respectively. *B*, colocalization (proximity) analysis between MCU and RyR2 IF (*top* bar chart) and between MCU and mtHsp70 (*bottom* bar chart) based on nearest neighbor distance ranges. The scheme illustrates approximate particle sizes (corresponding to fluorophores conjugated to individual antibodies). $n = 3$ mice; technical replicates, 5 cells each. *Error bars*, S.E.

mitochondrial fraction. To this end, the relative abundance of different mitochondrial proteins was determined in SR and mitochondrial fractions of rat and mouse heart homogenates. As shown in Fig. 8, *B* and *C* (rat) and *D* and *E* (mouse), SR-resident proteins calsequestrin and calnexin were strongly enriched in the SR fraction, whereas some IMM and matrix proteins (Tim23, NCLX, and mtHsp70) were enriched 2-fold to severalfold in the mitochondrial fraction. Strikingly, the mandatory mtCU component EMRE and the cristae junction constituent mitofilin/Mic60 were strongly (≥2-fold) enriched in the SR fraction, in line with the idea that the more "SR-wrapped" mitochondria in the SR fraction hosted more mtCU. Notably, a substantial pool of mitochondrial proteins displayed no or <50% (1.5-fold) enrichment in either fractions. MCU was falling in this pool with just slightly (not significantly) higher abundance in the rat heart mitochondrial fraction (Fig. 8, *B* and *C*). MICU1 enrichment among the fractions of mouse heart followed that of MCU (Fig. 8, *D* and *E*). MICU1 was tested only for the mouse tissue, where the antibody specificity could be referenced by MICU1 KO (25).

Interestingly, the enrichment of EMRE and mitofilin/Mic60 in the cardiac SR fraction relative to the mitochondrial fraction was more conspicuous in mice than it was in the rat (Fig. 8, compare *B* and *C* with *D* and *E*). On the other hand, when the crude mitochondrial and SR fractions of skeletal muscle (rat hind limb) were compared, both EMRE and MCU were enriched in the mitochondrial fraction to similar extents (Fig. 8, *F* and *G*). The extent of enrichment in the skeletal muscle mitochondrial *versus* SR fraction for EMRE and MCU was still much smaller than for mtHsp70 (>40-fold), suggesting that there was contamination of the SR by mitochondrial derivatives but without particular concentration of EMRE or MCU to them (Fig. 8, *F* and *G*).

The notion that MCU abundance was not higher in the SR *versus* the mitochondrial fraction led us to speculate that a significant portion of the MCU could have still located to SR-associated areas in the (crude) mitochondrial fraction. Indeed, isolation of mitochondria-associated reticular membranes (MAMs) is frequently done by separating the crude mitochondrial fraction on a Percoll gradient into a "light" (MAM-enriched) and "heavy" (purified mitochondrial) band (26). We thus decided to compare the protein abundance profiles of the SR *versus* crude mitochondrial *versus* Percoll-purified mitochondrial fractions (Fig. 9). As expected, SR-resident calsequestrin levels were severalfold lower in Percoll-purified *versus* crude mitochondrial fractions (Fig. 9, *B* (*i*) and *C*). Strikingly, the Percoll purification that diminished the SR-resident protein content also significantly reduced the MCU levels (Fig. 9*B*, *ii*), thus turning the direction of enrichment toward the SR fraction (Fig. 9*C*, note the crude mitochondrial fraction-directed downward deflection for MCU in the *top panel versus* the SR fraction-directed upward deflection in the *bottom panel*). This way the ratio of MCU abundance in the SR *versus* the Percoll-purified mitochondrial fraction became similar to that of VDAC (Fig. 9*C*). EMRE levels also decreased significantly upon Percoll purification of the mitochondrial fraction (Fig. 10*B*, *iii*). On the other hand, IMM-resident prohibitin levels displayed higher values in the Percoll-purified *versus* crude mitochondrial frac-

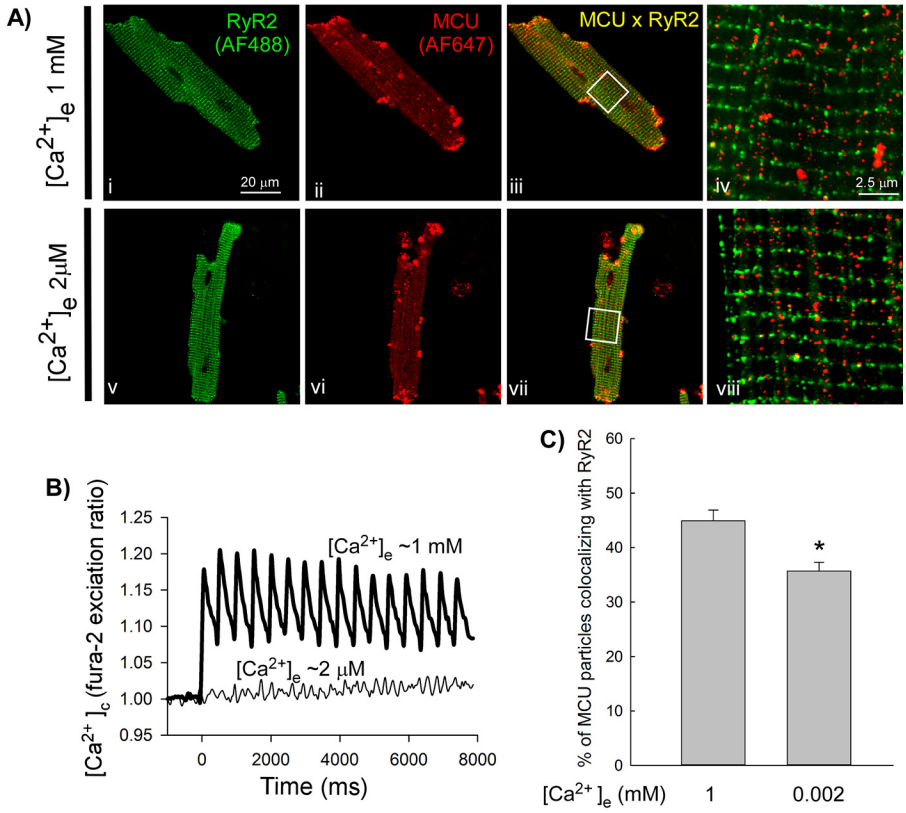

FIGURE 6. **Ca^{2+} signaling activity promotes MCU recruitment to dyad (RyR2) areas.** Colocalization of MCU and RyR2 fluorescence was determined in adult cardiomyocytes that were perfused with (1 mM) or quasi-without (2 μM) Ca^{2+} and field-stimulated for 10 min (2 Hz) before fixation. *A*, representative Airyscan images of MCU and RyR2 IF (*labeled* as in Fig. *4B*) in representative cardiomyocytes ($[Ca^{2+}]_e$ ~1 mM in *i–iv* (*top*), ~2 μM in *v–viii* (*bottom*)). Overviews (*i–iii* and *v–vii*) and enlargements (*iv* and *viii*) are organized as in Fig. *4B*. *B*, representative $[Ca^{2+}]_c$ (excitation ratio of fura-2 loaded as fura-2/AM) recordings from two cardiomyocytes paced at $[Ca^{2+}]_e$ ~1 mM (*thick line*) or ~2 μM (*thin trace*). *C*, percentage of MCU IF colocalization with RyR2 determined the same way as in Fig. 4*C*. $n = 3$ mice; technical replicates, 2 coverslips/mouse, 5 cells from each. *Error bars*, S.E. *, $p \leq 0.05$.

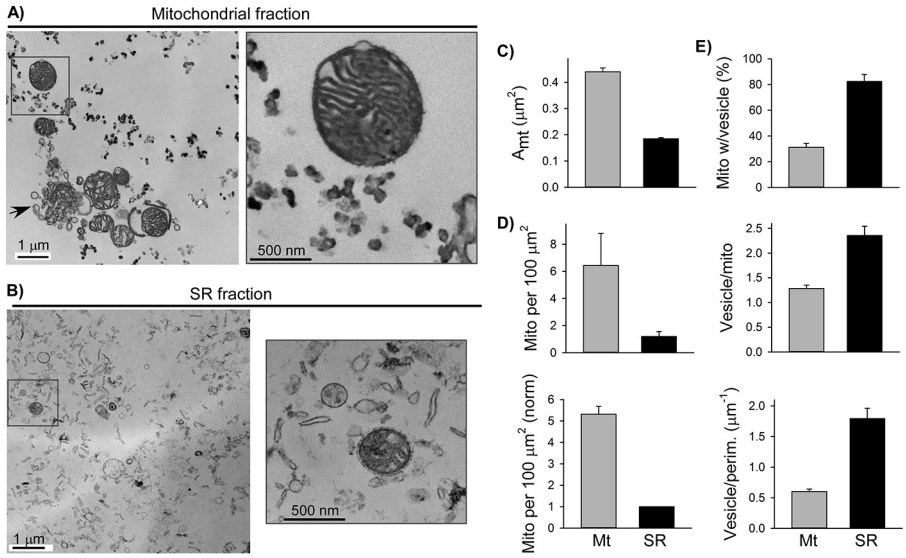

FIGURE 7. **Ultrastructural differences between SR and mitochondrial fractions.** *A* and *B*, representative transmission electron micrographs of the organelles and membrane vesicles/particles in sections of high pressure frozen suspensions of mitochondrial (*A*) and SR (*B*) fractions at equal protein concentration. Note that the structures are not crammed together because they were not processed as an ultracentrifuge pellet. *Left*, bar graphs show the average individual cross-section area (*C*) and quantity (count/100 μm^2) (*D*) of well defined mitochondria from two independent preparations. Bar graphs in (*E*) quantitate mitochondrial association with membrane vesicles in one of the preparations in terms of the fraction of the mitochondrial count displaying vesicle association (*top*), the average (≥0) number of vesicles associated with a single mitochondrion (*middle*), and the average number of vesicle associations per mitochondrial perimeter (*bottom*) for 220 and 79 mitochondrial cross-sections in mitochondrial and SR fractions, respectively ($n = 2$ rats). *Error bars*, S.E. *, $p \leq 0.05$.

tion (Fig. 9*B*, *iv*). Although the mean density values themselves were not significantly different, the extent by which they surpassed the prohibitin levels in the SR fraction was significantly larger in the Percoll-purified mitochondria (normalized density differences 0.32 ± 0.1 *versus* 0.11 ± 0.07, means ± S.E., $n = 3$, $p < 0.05$).

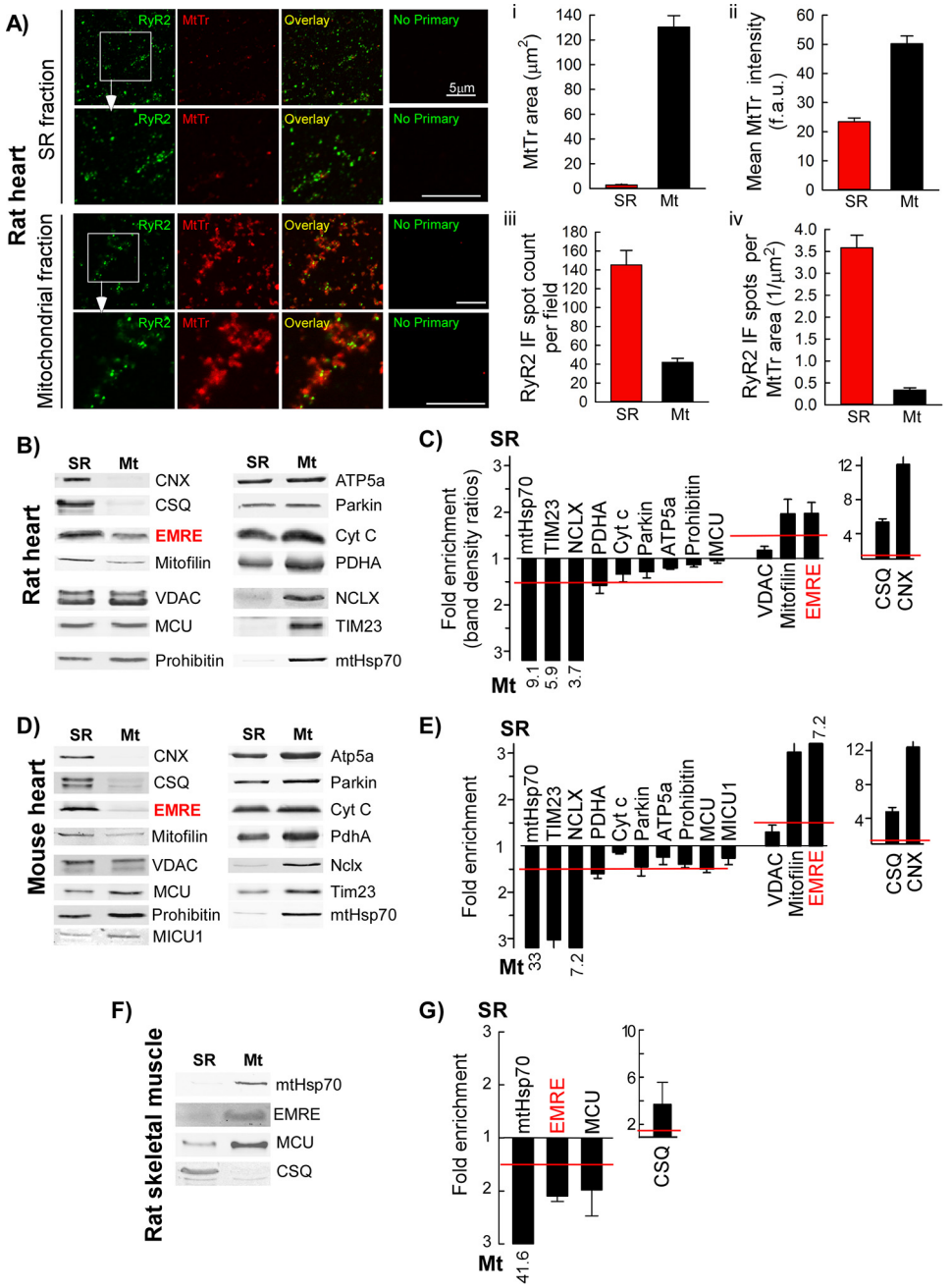

FIGURE 8. **Mitochondrial content in SR and mitochondrial fractions differ in their protein profile and membrane (jSR) associations.** *A*, anti-RyR2 IF (AF 488; *green*) and MtTrRed (MtTr; *red shades*) distribution in glass-mounted SR and mitochondrial fractions (as labeled). Bar graphs show the MtTrRed fluorescence area per field (*i*), the mean (per pixel) fluorescence intensity of MtTr (*red*) that is determined by the $\Delta\Psi_m$-dependent loading of the dye (*ii*), the number of all anti-RyR2 IF spots per field (*iii*), and the number of colocalizing anti-RyR2 IF spots per area unit of MtTrRed fluorescence (*iv*). Note that whereas the number of RyR2 IF spots is <4 times more in the SR fraction (145 ± 15 *versus* 42 ± 4.5), the number of colocalizing RyR2 spots per MtTrRed area unit is over 10-fold more in the SR fraction (3.6 ± 0.3 *versus* 0.34 ± 0.05 per μm^2 of MtTr). $n = 3$ rats; technical replicates, 3–4 each. *B*, representative WB of various mitochondrial and SR resident proteins in SR and mitochondrial fractions isolated from rat heart. *NCLX*, mitochondrial $Na^+/Li^+/Ca^{2+}$ exchanger; *PDHA*, pyruvate dehydrogenase E1 component subunit α; *Cyt c*, cytochrome *c*; *ATP5a*, ATP synthase subunit α; *CNX*, calnexin. *C*, relative (-fold) enrichment of the respective proteins in the mitochondrial (*downward deflection*) and SR (*upward deflection*) fractions expressed as the ratio of the WB band densities (higher divided by lower). A value of 1 would represent equal band densities between mitochondrial and SR fractions. *Red lines* demarcate 1.5-fold enrichment. Values exceeding the axis range are shown at the *tip* of the corresponding *bar*. *Panels D* and *E* and *panels F* and *G* show similar comparative results as *B* and *C* from mouse heart and rat skeletal muscle homogenates, respectively. $n = 4$ rats and 4 mice for heart, 2 rats for skeletal muscle. *Error bars*, S.E.

Collectively, these data suggest that in the cardiac muscle mitochondria, both functionally mandatory mtCU constituents EMRE and MCU concentrate to the mitochondria-jSR associations but to a different extent, with EMRE displaying stronger preference for the extensively SR-associated mitochondria in the SR fraction. Also, the contact points aligned with the interface with jSR (22) might have a distinct composition (*e.g.* host more EMRE and mitofilin). This arrangement is not apparent in the skeletal muscle, in which mtCU expression levels are high (21) and the Ca^{2+} release units (triads) are more distant from the mitochondrial surface (27).

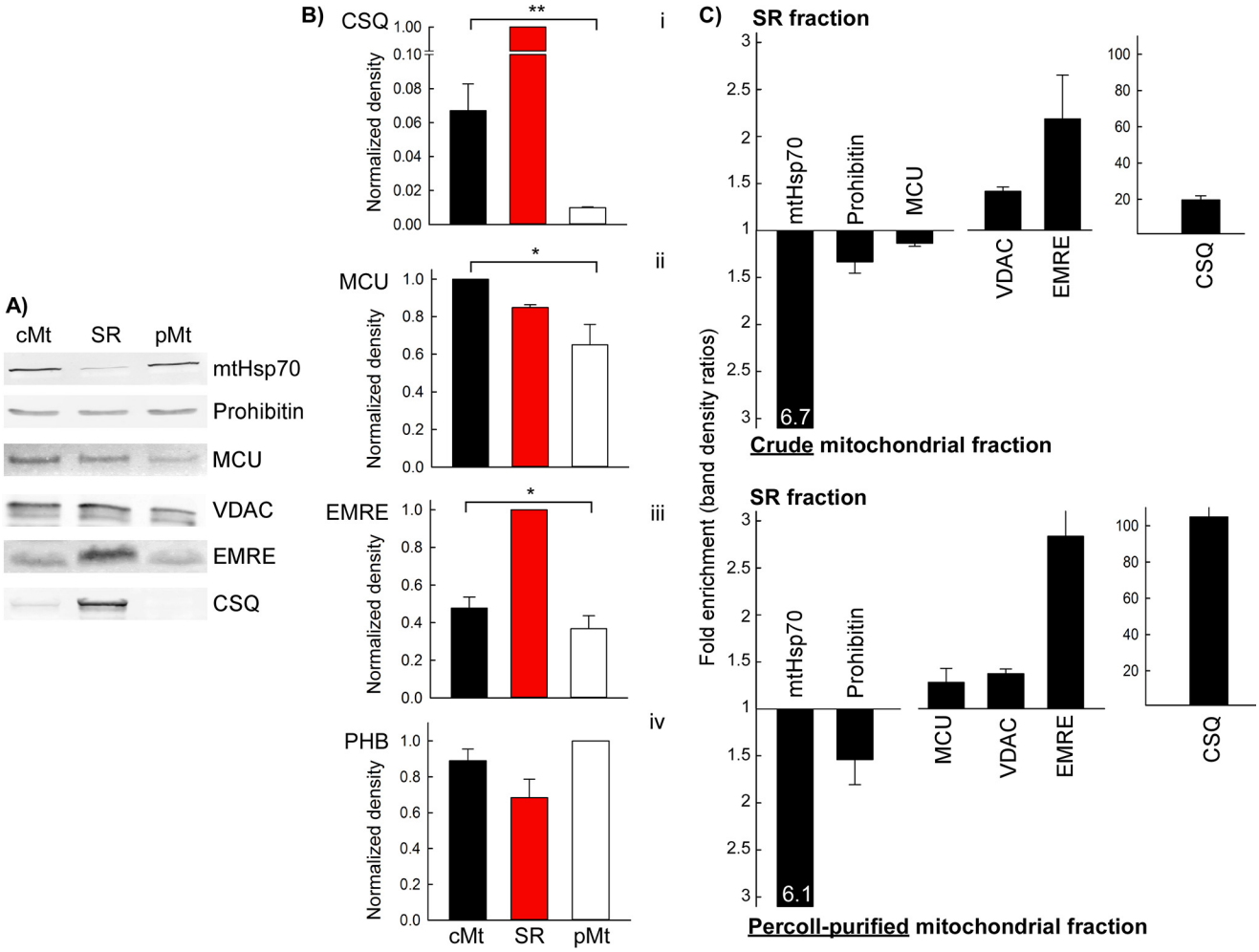

FIGURE 9. **Percoll purification decreases MCU and EMRE levels in the mitochondrial fraction.** In similar comparative assays as in Fig. 8, mitochondrial and (for reference) SR protein levels were compared between crude and Percoll-purified mitochondrial fraction as well as the SR fraction isolated from rat heart. *A*, representative WB of mitochondrial and SR-resident proteins in the three fractions as labeled (*cMt* and *pMt* are crude and Percoll-purified mitochondrial fractions, respectively). *B*, bar charts showing the the relative abundance of the SR-resident calsequestrin (*i*) and the mitochondrial proteins MCU (*ii*), EMRE (*iii*), and prohibitin (*iv*). *C*, -fold enrichment for all proteins analyzed in SR *versus* crude mitochondrial (*top*) and SR *versus* Percoll-purified mitochondrial (*bottom*) fractions expressed as abundance ratios as in Fig. *8C*. $n = 3$ rats. *, $p \leq 0.05$; **, $p \leq 0.01$.

MCU and EMRE Contribute to Differently Sized Complexes in the SR and Mitochondrial Fractions—The higher enrichment of EMRE than MCU in the SR fraction raised the possibility of differential molecular composition of the mtCU complex inside and outside the area of mitochondria-jSR associations. To this end, protein complexes from non-denaturing detergent-solubilized mitochondrial and SR fractions had been separated via size exclusion (gel filtration) chromatography, and their MCU and EMRE content profiles were established. Of the 22 fractions collected, fraction 9 corresponded to the void volume, where large molecules completely excluded from entering the column beads were eluted. For a crude reference (separation is based on size and shape, not mass), the ~2-MDa blue dextran elutes in this fraction, whereas the ~450-kDa apoferritin complex elutes at fraction 17 (*arrows* in Fig. 10*B*). The MCU content profile of the variously sized complexes was multimodal in both mitochondrial and SR fractions. In the SR fraction, a steep rise to a plateau of maximum abundance (75–100%) at the void volume (fraction 9) was followed by a steep decline to <20% from fraction 14 to 18 (Fig. 10*B*, *red trace*). In the mitochondrial fraction, on the other hand, maximum MCU abundance was reached in a peak at fraction 10 with the neighboring fractions containing ~45% abundance levels, and from there it gradually decreased to 23% by fraction 20, after which it dropped to its minimum (Fig. 10*B*, *black trace*). The EMRE content profile of the differently sized complexes in the SR fraction closely followed the MCU content profile throughout the fractions (Fig. 10, *C* and *D*, *red traces*). By contrast, the EMRE content profile of the complexes from the mitochondrial fraction was unimodal. The peak was closely overlapping with the MCU peak but steeply diminished down to <8% abundance levels by fraction 14 (Fig. 10*C*, *black*), thus strongly diverging from both the MCU profile of the mitochondrial fraction (Fig. 10*D*, *black traces*) and EMRE profile of the SR fraction (Fig. 10*C*, *black versus red*). Overall, these observations suggest the following. (i) The principal constituents of the mtCU complex, MCU and EMRE, appear in a wide range of differently sized protein complexes, with a substantial portion being built into very large complexes, probably in or close to the 10^6 Da range. (ii) Importantly, for the SR fraction, the MCU content and

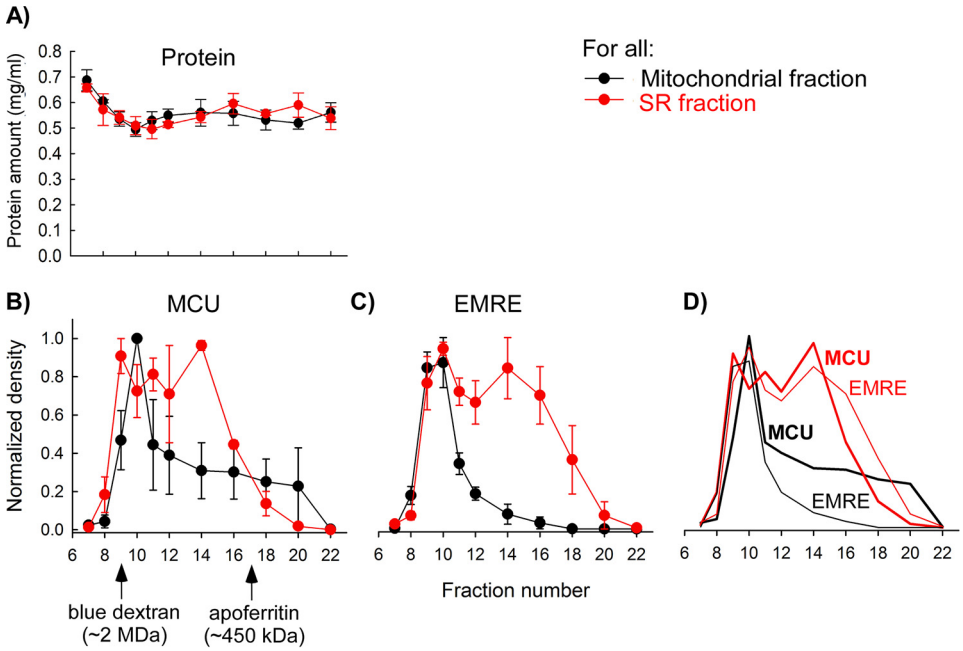

FIGURE 10. **Size profiles of MCU and EMRE-containing macromolecular complexes in mitochondrial and SR fraction.** Size exclusion (gel filtration) chromatography profiles of MCU and EMRE were established from non-denaturing detergent (CHAPS) lysates of mitochondrial (*black*) and SR fractions (*red*). The *smaller* the *fraction number*, the larger is the size of the complexes. For reference (*arrows*), fraction 9 corresponds to the void volume (where complexes are usually $>10^6$ Da), whereas the ~450-kDa apoferritin peaks in fraction 17. *A*, protein profile of the MCU and EMRE-containing fractions. *B–D*, abundance of MCU (*B*) and EMRE (*C*) in the fractions as determined by WB and normalized to the band intensity range. Line plots from *B* and *C* are overlaid in *D*. Note that EMRE follows MCU throughout the size range in SR but not in the mitochondrial fraction, where it is unrepresented or underrepresented in the smaller complexes. $n = 3$ rats. *Error bars*, S.E.

EMRE content profiles are similar over the resolved size range of complexes, whereas for the mitochondrial fraction, MCU and EMRE contents diverge toward the smaller sized complexes, some of which may contain MCU but lack EMRE. Hence, a part of the pool of MCU outside the mitochondria-jSR association area may exist in (relatively small) functionally compromised or silent complexes that incorporate suboptimal or no EMRE.

mtCU-mediated Ca^{2+} Uptake Is More Effective into the Mitochondria of the SR Fraction—To test whether the above identified biases in MCU and EMRE distribution impacted mtCU function, mitochondrial $^{45}Ca^{2+}$ isotope uptake assays were carried out in suspensions of mitochondrial and SR fractions isolated from the rat heart. As mentioned before (Fig. 7, *A–D*), the SR fraction contained fewer and smaller mitochondria per total protein. Cristae details also appeared less sharply defined in the mitochondria of the SR fraction (*e.g.* compare the *enlarged images* in Fig. *7A versus* those in Fig. 7*B*). $\Delta\Psi_m$-dependent accumulation of MtTrRed appeared also weaker in the coverglass-attached mitochondria of the SR fraction (Fig. 8*A*, *bar chart ii*). For comparative assessment of mtCU activity, compensation had to be applied for these differences. Activity assays for the matrix enzyme, citrate synthase, have been commonly utilized as a quantitative reference for the content of intact mitochondria in suspensions. Respiratory enzyme assays are frequently normalized to the citrate synthase activity (*e.g.* see Ref. 28). We thus decided to normalize the measured mtCU-mediated Ca^{2+} uptake activities to the citrate synthase activities in the SR and mitochondrial fractions.

MtCU-mediated Ca^{2+} uptake was defined as the Ru360-sensitive Ca^{2+} accumulation at pharmacologically blocked mitochondrial Ca^{2+} efflux pathways and disabled/depleted SR Ca^{2+} store. The initial uptake was determined after elevating $[Ca^{2+}]_o$ by a pretitrated $CaCl_2/^{45}CaCl_2$ bolus for 15 s. The titration was done by cuvette fluorometry using the ratiometric high and low affinity indicators Fura-2 and Fura-loAff. Recent direct Ca^{2+} measurements in the dyadic cleft of rat cardiomyocytes estimated local systolic $[Ca^{2+}]_c$ peaks inside the clefts to be ≥1.1–1.5 μM (29). This was used as crude estimate for the local $[Ca^{2+}]$ peak in the mitochondria-jSR cleft (which is supposed to be smaller than in the dyadic cleft, given the larger distance from RyR2s). Two $[Ca^{2+}]_o$ levels were tested: ~300 nM and ~1.5 μM. Most of the initial Ca^{2+} accumulation happened via mtCU with a relatively small Ru360-insensitive component (Fig. 11*A*). Without correction, initial Ca^{2+} accumulation at $[Ca^{2+}]_o$ ~1.5 μM was significantly greater in the mitochondrial fraction (1.61 ± 0.11 *versus* 0.76 ± 0.11 nmol/mg protein; Fig. 11*B*), whereas at $[Ca^{2+}]_o$ ~300 nM, the difference was negligible. Citrate synthase activity was on average ~7.5 (7.55 ± 0.6, $n = 4$)-fold higher in the mitochondrial than in the SR fraction at equal total protein concentrations (Fig. 11*C*, *left*). This -fold difference, individually determined for each experiment, was used as the correction factor for the mitochondrial Ca^{2+} uptake. For reference, increasing the total protein of the SR fraction by 10-fold increased its citrate synthase activity level proportionally, slightly surpassing that in the mitochondrial fraction (Fig. 11*C*, *ii* (*red bar*) *versus i* (*black bar*)). Increasing the total protein of the mitochondrial fraction by 10-fold using heat-inactivated (boiled) suspension did not change significantly its citrate synthase activity (Fig. 11*C*, *i versus ii* (*black bars*)). IMM integrity was also assessed by measuring the portion of citrate synthase activity that did not require membrane

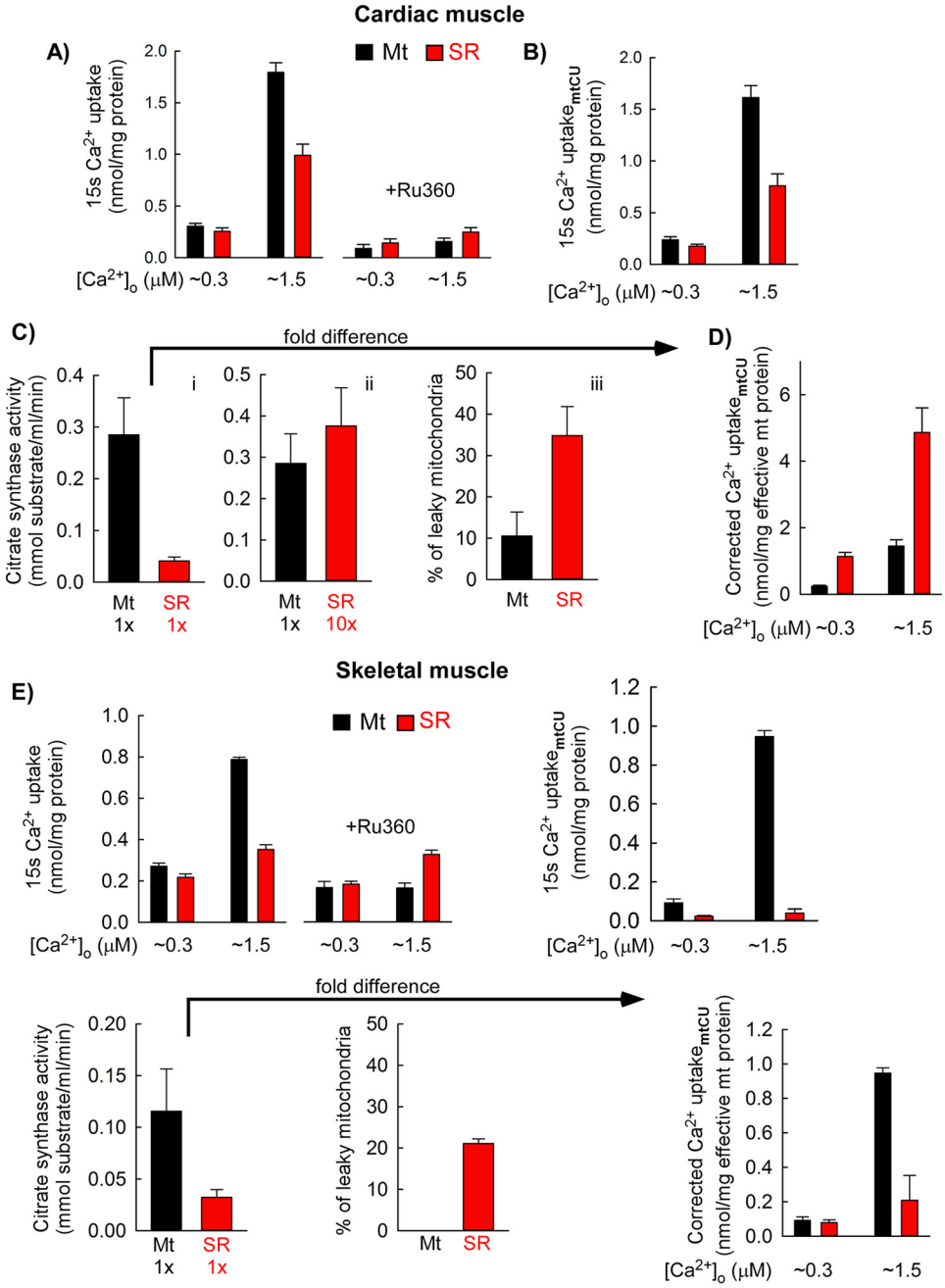

FIGURE 11. **Greater mitochondrial Ca^{2+} uptake efficacy in the SR fraction than in the mitochondrial fraction of the cardiac but not skeletal muscle.** Ca^{2+} uptake assays based on $^{45}Ca^{2+}$ isotope retention. Ca^{2+} uptake activation was determined from the initial (15-s) $^{45}Ca^{2+}$ accumulation in suspensions of mitochondrial (*Mt*; *black*) and SR (*SR*; *red*) fractions of cardiac (*A–D*) and skeletal (*E*) muscle. The SR Ca^{2+} store was depleted, and SR Ca^{2+} uptake and mitochondrial Ca^{2+} extrusion pathways (mitochondrial Na^+/Ca^{2+} exchanger and the permeability transition pore) were pharmacologically blocked (by thapsigargin, CGP-37157, and cyclosporine A, respectively). *A*, initial Ca^{2+} uptake at $[Ca^{2+}]_o$ ~0.3 and ~1.5 μM in the absence (*left*) and presence (*right*) of Ru360 (10 μM) in cardiac mitochondrial and SR fractions. *B*, mtCU-mediated (Ru360-sensitive) initial Ca^{2+} uptake (Ca^{2+} $uptake_{mtCU}$) calculated from *A*. *C*, citrate synthase activity in the mitochondrial and SR fractions at equal protein amount per assay (*left*) or, for reference, with 10 times more unaltered protein in the SR than in the mitochondrial fraction (*middle*). In the latter case, to maintain equal proteins, the unaltered mitochondrial fraction was supplemented with nine portions of heat-denatured/boiled mitochondrial fraction. *Right*, percentage portion of citrate synthase activity in the two fractions that did not require membrane permeabilization, corresponding to mitochondria with compromised IMM integrity (leaky/broken mitochondria). *D*, initial Ca^{2+} $uptake_{mtCU}$ adjusted by the -fold difference in citrate synthase activity per total protein between the mitochondrial and SR fractions (from *C*, as the *arrow* shows). *E*, the same experiments as in *A–D* were done using skeletal muscle mitochondrial and SR fractions. For all, $n = 3$ rats; 3 technical replicates for each point. *Error bars*, S.E.

permeabilization. This portion ("leaky mitochondria") was ~20% in the mitochondrial, whereas it was ~55% in the SR fraction (Fig. 11*C*, *iii*); this -fold difference was not included in the correction to avoid overshooting. After correcting to the relative citrate synthase activities, the initial Ca^{2+} uptake into the mitochondria of the SR fraction became significantly larger than that into the mitochondria of the mitochondrial fraction at both tested $[Ca^{2+}]_o$ levels (0.23 ± 0.03 *versus* 1.13 ± 0.12 and 1.45 ± 0.18 *versus* 4.86 ± 0.74 for $[Ca^{2+}]_o$ ~300 and ~1.5 μM, respectively; Fig. 11*D*).

The same assays were also performed using mitochondrial and SR fractions of the skeletal muscle, in which EMRE and MCU were both strongly enriched in the mitochondrial fraction (Fig. 8, *F* and *G*). By strong contrast to the cardiac muscle, the mtCU-mediated initial mitochondrial Ca^{2+} uptake was severalfold larger at $[Ca^{2+}]_o$ in the micromolar range even after correcting to the difference in citrate synthase activities (which was smaller than in the heart, 3.4 ± 0.75-fold) (Fig. 11*E*).

Together, these functional assays are consistent with more extensive jSR-associated mitochondrial regions in the cardiac muscle SR fraction to host mtCU in higher density and/or with more competence than those in the mitochondrial fraction with less associated jSR. Such functional bias is not present in the skeletal muscle, where the mtCU components EMRE and MCU are not concentrated to the SR-associated mitochondrial segments.

Discussion

We tested the hypothesis that in cardiac muscle, mitochondria mtCU-mediated Ca^{2+} uptake activity is biased toward the mitochondria-jSR associations, the sites of local exposure to RyR2-derived Ca^{2+} signals. Multiple levels of biases were found when the distribution of the essential channel constituents MCU and EMRE were interrogated. Both proteins displayed preference for the contact points and inner boundary membrane as opposed to being deep in the cristae folding, as resolved via membrane fractionation and super-resolution approaches in both isolated mitochondria and freshly isolated primary cardiomyocytes. mtCU in some non-muscle cells has been proposed to also operate inside the cristae so that opening and tightening cristae junctions would regulate mtCU exposure to Ca^{2+} signals (30, 31). Such topology in adult myocardial mitochondria would require a lot of mtCU to populate all of the numerous cristae for an effective local Ca^{2+} signal reception. This seems unlikely, because mtCU current densities in cardiac mitoplasts have been measured to be the lowest of a large range of mouse tissues (21). Being placed close to the cyto/sarcoplasmic boundary presumably offers mtCU better exposure to Ca^{2+} entering the intermembrane space.

The immunovisualization approaches to resolve mtCU distribution were focused around anti-MCU IF. Suitable EMRE antibody for IF and knock-out animals for tissue-specific verification are still awaited. Homogenous mitochondrial membrane distribution of anti-MCU IF has been recently reported in rabbit cardiomyocytes (32). All of our cellular models (rat and mouse ventricular myocytes, MEFs, HeLa) showed clustered anti-MCU labeling over individual mitochondria. Also, the antibody used in the referenced work (Sigma HPA016480) produced strong nonspecific cross-labeling all across the cytoplasm of MCU KO cardiomyocytes so that we could use it only to label isolated mitochondria. Here we validated another MCU antibody (CST D2Z3B) that has been used before to determine MCU expression levels in cardiac muscle but not for IF (18), and it performed well across the bulk of the sarcoplasmic area. Immunofluorescent particle analysis using various confocal and super-resolution/single-molecule imaging of crude mitochondrial fraction or freshly isolated cardiomyocytes found ~50 ± 5% of the MCU colocalized with RyR2. We interpret this as a distribution bias, considering that the mitochondrial interface formation with dyad(s) in most of the cases engages less than one-third of the entire mitochondrial surface. For this, the resolution had to be sufficient to distinguish anti-MCU IF spots along the four cardinal directions over a mitochondrion. Even with the confocal microscope, the mean anti-MCU IF particle area was >10-fold smaller than that of the diffusely distributed MtTrRed or cytochrome *c*, thus sufficiently small to resolve a polarized distribution.

Originally, MCU was suggested to exist in a ~480-kDa complex (33) that still remained close to 400 kDa upon ablation of EMRE (3). Higher molecular mass (~720 kDa) complexes have also been described, and their existence depends on EMRE and MICU1/2 (3, 4, 34). Consistently, size exclusion chromatography suggested very large complexes incorporating a major portion of the MCU and EMRE pool to be on a par with the blue dextran (2 MDa). Nevertheless, MCU contributed to a wide size range of complexes, some of which were clearly smaller than the originally predicted size of the "uniplex" (~480 kDa, which would probably correspond to fractions 16 and 17 of the 22, based on where the apoferritin complex of similar molecular mass elutes). The precise molecular composition and stoichiometry of this wide size range of MCU-containing complexes remain to be elucidated. Nevertheless, the lack or diminishment of EMRE was characteristic of smaller complexes in the mitochondrial fraction. This probably reflected the proposed role of EMRE to connect MICU1/2 oligomers to the mtCU complex (3) via its C-terminal acidic tail in the intermembrane space (5, 7). Without EMRE or MICU1, MCU has been shown to stay in a ~300-kDa complex (3) that might correspond to MCU-containing complexes from the mitochondrial fraction eluted in fractions 18 and 19. Considering the recently revealed pentameric structure, the MCU oligomer without any accessory proteins would be ~175 (5 × 35) kDa (35). Because size exclusion fractions cannot be directly translated to molecular mass ranges, it would be difficult to tell if the end of the size range (fraction 20) could correspond to this pentamer. Loss of MICU1/2 has been connected to enhancement of basal channel activity because of impaired gatekeeping and decreased $[Ca^{2+}]$ activation threshold (34, 36–38). Nevertheless, in vertebrates, the channel activity itself fundamentally requires EMRE (3–6), without which the presence or absence of other regulatory subunits becomes functionally irrelevant. In any case, with the notion that one of the recently proposed functions of EMRE is to retain MICU1 (5), one would expect MICU1 to follow EMRE in its distribution pattern. When MICU1 relative abundance was determined for the mitochondrial and SR fractions, it was similar to MCU, not EMRE. However, because the overall mitochondrial membrane integrity was more compromised in the SR fraction, as revealed by the citrate synthase assays and electron microscopy, the possibility cannot be excluded that a portion of this peripheral/membrane-associated protein of the intermembrane space had been lost during preparation (to a larger extent from the SR fraction). Regardless, because MICU1 seems to have the ability to bind individually to both MCU and EMRE (5), it is not mandated to EMRE-containing complexes only. Thus, further studies with alternative approaches will be needed to establish the potential location-specific contri-

bution of MICU1 to the mtCU complex in cardiac muscle mitochondria.

A large portion of the imaging, biochemical, and functional assays presented here to capture the bias(es) in mtCU distribution relied on comparing mitochondrial and SR or submitochondrial fractions. Fig. 12 shows our mechanistic model of how recruitment of EMRE-complemented competent but not EMRE-deprived incompetent MCU complexes to the mitochondria-jSR association area would explain the experimental observations. As shown in Fig. 12 (*top*), mitochondria in the cardiomyocyte may exist in various shapes/sizes with or without an interface with a dyad. Mechanical homogenization of the ventricular wall yields various mitochondrial and SR formations (Fig. 12, *middle*). Some mitochondria may exit the tissue without major structural alteration (*Whole*). Some, especially larger ones or those interconnected via "nanotunnels" (39) could undergo fragmentation (*Fragmented*). Others may rupture, yielding various IMM-, OMM-, and IMM-OMM-SR-containing (submitochondrial) vesicles (*Ruptured*). When this homogenate is subjected to differential centrifugation (*bottom*), extensive jSR associations would make smaller mitochondria (whole or derived from fragmented larger ones) more buoyant and so sediment in the SR fraction. These mitochondria with a large surface portion interfacing with jSR would harbor high levels of competent MCU per mitochondrial protein. Larger "whole" mitochondria with a smaller segment of their surface associated with jSR and mitochondria without a jSR connection would sediment in the mitochondrial fraction and host competent mtCU complexes at the jSR association area and miscellaneous complexes outside of it. We consider complete (whole or fragmented) mitochondria as the main Ca^{2+}-handling mitochondrial elements in the suspensions, although some contribution of submitochondrial IMM vesicles from ruptured mitochondria was also likely in both fractions.

Verification of biased mtCU-mediated Ca^{2+} uptake activity at the submitochondrial level *in situ* in a permeabilized cardiomyocyte is difficult due to various tightly packed Ca^{2+} diffusion limiters (*e.g.* sarcomeres, Ca^{2+} binding sites at/around the mitochondria-jSR interface) that may interfere with globally applied Ca^{2+} to uniformly expose the mitochondrial surface. T-tubules also tend to be less sensitive to permeabilization (40); thus, the added Ca^{2+} may better access the bulk of the sarcoplasm than the mitochondrial interface with dyads. Recently, in paced rabbit cardiomyocytes, $[Ca^{2+}]_m$ signals were found larger at the Z lines (where dyads locate) than at the M lines (32), indicating effective local mitochondrial Ca^{2+} uptake.

The molecular mechanism(s) that drives MCU and even more EMRE to the mitochondria-jSR association area remains to be elucidated in its entirety. Importantly, here we identified the Ca^{2+} signaling activity as a significant factor in recruiting MCU into close proximity with RyR2 in freshly isolated ventricular myocytes. Further studies will be needed to identify the Ca^{2+} sensor that would mediate the recruitment. Potential candidates could be the acidic tail of EMRE, which has been proposed to be analogous to Ca^{2+}-sensing motifs ("Ca^{2+} bowl" and "Ca^{2+} clasp") of some ion channels (6) and the EF-hand regulatory proteins MICU1/2. One would also expect direct or indirect contribution by mitochondria-jSR tethers that secure the organelles together. Cardiac ablation of mitofusin 2, a multifunctional OMM protein that has been proposed to be (41) or not to be (42, 43) a mitochondria-ER tether in non-muscle cells, causes a decrease in mitochondria-jSR associations and Ca^{2+} transfer, suggesting a tethering role in cardiomyocytes (44). However, the -fold enrichment of EMRE in the SR *versus* mitochondrial fractions was not affected significantly by cardiac mitofusin 2 ablation ($n = 4$ mice), suggesting that either EMRE recruitment to the mitochondria-jSR association did not require mitofusin 2 or alternative mechanism(s) compensated for its loss. Of note, EMRE and mitofilin/Mic60, the two IMM proteins found strongly enriched in the SR fraction in our assays, are both single-pass transmembrane proteins, and as such, they probably share membrane insertion (*e.g.* stop-transfer) (45) and possibly degradation pathways. Because Tim23 and mtHsp70 proteins that assist IMM insertion (45) were highly enriched in the mitochondrial fraction, a location bias in the IMM insertion of EMRE and mitofilin toward mitochondria-jSR association is not likely. Further studies will be needed to evaluate whether the mitochondria-jSR association area could be protective against EMRE degradation or to elucidate possible other mechanisms underlying the strategic mtCU positioning. Because many mitochondrial membrane proteins are multifunctional (*e.g.* mitofusin 2 in the OMM, Letm1, MCUR1 in the IMM), a possibility remains that the disproportionally high enrichment of EMRE *versus* MCU in the SR-associated mitochondrial regions might also serve yet to be identified role(s) for EMRE other than being an mtCU constituent.

Strategic mtCU positioning that we have found here in the cardiac muscle of rat and mouse is not necessarily a ubiquitous phenomenon for the mitochondrial-reticular associations that serve local Ca^{2+} transfer. An arrangement that makes biological sense at low mtCU abundance, large mitochondrial size, and extensive cristae folding in the cardiac muscle might make no sense in other tissue like skeletal muscle with high channel abundance (21), smaller mitochondria, less extensive cristae, and larger distance (>100 nm (46)) between RyR and the mitochondrial surface. Indeed, when mitochondrial and SR fractions isolated from skeletal muscle of rat were compared, EMRE showed no enrichment in the SR as it did in the cardiac muscle; instead, it showed enrichment in the mitochondrial fraction similar to that of MCU (~2-fold). Consistently, in the mtCU-mediated mitochondrial $^{45}Ca^{2+}$ uptake assays, the mitochondria of skeletal muscle SR fraction underperformed those of the mitochondrial fraction.

Collectively, here we present evidence for multiple levels of biases in the location and molecular composition of the mtCU in the cardiac muscle. Selective concentration of EMRE-complemented mtCU complexes to the area of jSR association would represent a Ca^{2+} uptake "hot spot" where the $[Ca^{2+}]$ nanodomains even at the 30–50-nm distance from the Ca^{2+} release units (RyR2s) (13) could effectively activate Ca^{2+} uptake and support excitation-energetics coupling. Meanwhile, outside the mitochondria-jSR association areas, the global $[Ca^{2+}]_c$ oscillations would expose a less effective, more dispersed mtCU population that is partly silent or impaired due to missing or suboptimal EMRE module(s), probably as a protective measure from overload, as has been proposed (21).

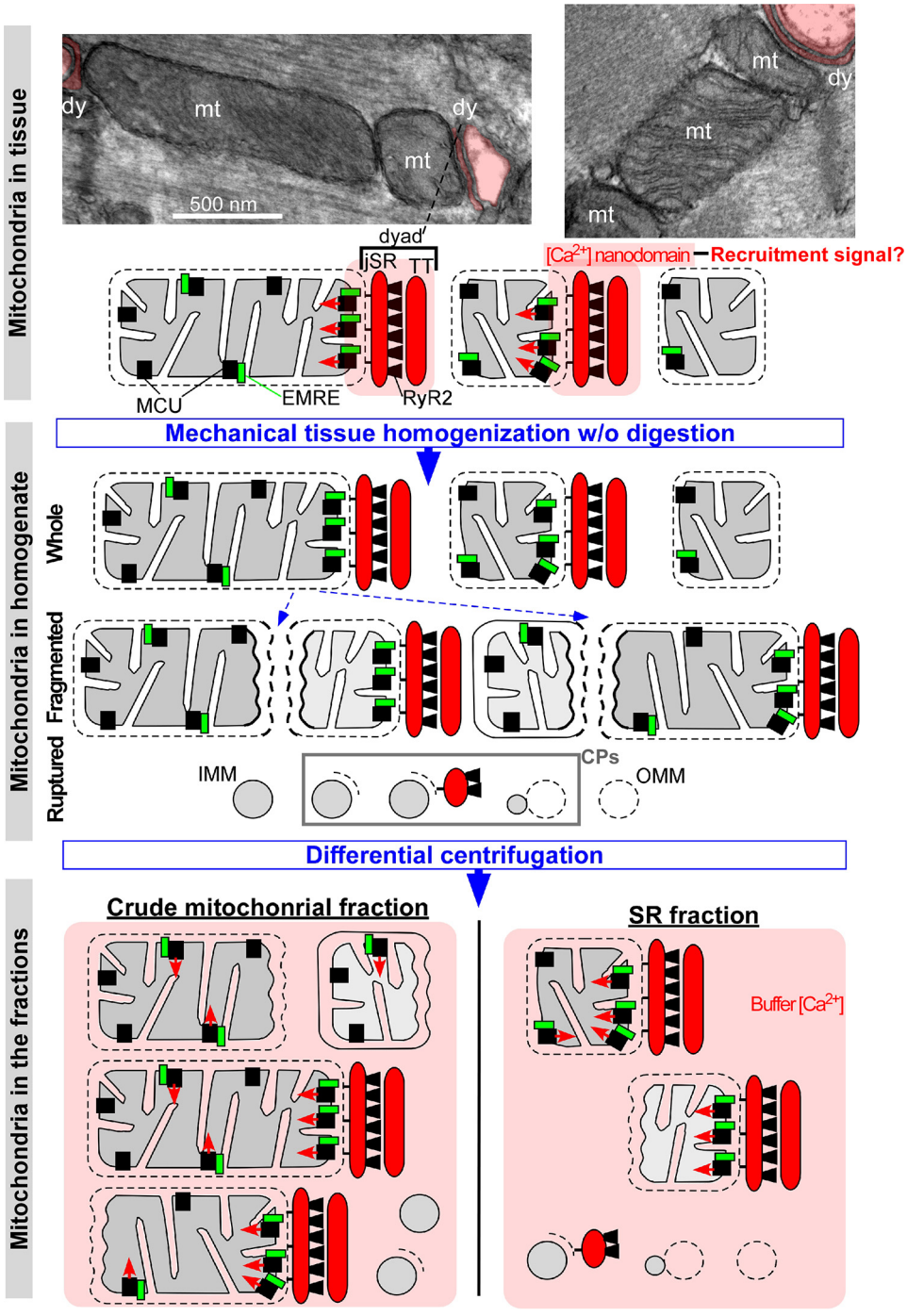

FIGURE 12. **Schematics for the mtCU distribution and activity bias toward mitochondria-jSR associations in the cardiac muscle and for the related differences between mitochondrial and SR fractions.** *Top* (*Mitochondria in tissue*), TEM images of rat ventricular wall segments illustrate the context of differently sized jSR-associated mitochondria (*mt*) in the tissue. Dyad (*dy*)-forming SR and T-tubule lumens are *shaded* in *light red* (two in the *left* and one in the *right image*). *Below*, two exemplary mitochondrion-jSR associations (involving either a small or a large mitochondrion) are depicted with the proposed bias in mtCU distribution and a third without dyad association. MCU complexes (*black rectangles*) complemented with EMRE (*green rectangles*) are more prevalent at the interface with the jSR, whereas mtCU lacking EMRE stays outside the interface. Hence, the short lasting RyR2-derived high $[Ca^{2+}]$ nanodomain (depicted as *light red shade*) exposes an IMM segment containing MCU at higher density and always complemented by EMRE. By contrast, diluted global $[Ca^{2+}]_o$ rises (not depicted) would expose IMM surfaces outside the dyad interface hosting MCU at smaller density, some of which may not be complemented by EMRE (and so incapacitated). The *middle* and *bottom panels* illustrate the potential fates of the mitochondria upon tissue homogenization and isolation via differential centrifugation of the mitochondrial and SR fractions, respectively. In the *bottom panel*, the mitochondrial derivatives in the two fractions are shown in an elevated $[Ca^{2+}]_o$ environment, and Ca^{2+} influx through the activated MCU is depicted by *red arrows* to explain the differences observed during the $^{45}Ca^{2+}$ uptake assays (Fig. 11). Although there are more active mtCU per mitochondrion in the SR fraction, those mitochondria are fewer (not depicted) with probably weaker $\Delta\Psi_m$ and more compromised membrane integrity (*paler gray shade* in the matrix). Membrane vesicles derived from mitochondrial rupture are also shown for both fractions but not shown as active in Ca^{2+} uptake because in many of them the $\Delta\Psi_m$ generation is probably compromised. See "Results" for more details.

Experimental Procedures

Materials—Chemicals and reagents were purchased from Sigma-Aldrich or Thermo Fisher Scientific unless otherwise specified. Reagents for transmission electron microscopy (TEM) preparations were from Electron Microscopy Sciences. The protein assay kits, Western blotting (WB) reagents, and Chelex 100 sodium were from Bio-Rad. Thapsigargin and CGP-37157 were from Enzo Life Sciences. Fluorescent Ca^{2+} indicator dyes (Fura-2 and Fura-loAff K^+ salts and fura-2 acetoxymethyl ester) were from Teflabs. The membrane potential dye tetramethylrhodamine methyl ester and MitoTraker®Red CMXRos were from Molecular Probes (Thermo Fisher Scientific). Primary antibodies were as follows (dilutions when not specified are for WB). Anti-VDAC rabbit polyclonal (ab15895, 1:800), anti-calsequestrin rabbit polyclonal (ab3516, 1:500), anti-prohibitin rabbit polyclonal (ab28172, 1:1000), anti-ATP5A mouse monoclonal (ab14748, 1:2000), and anti-mitofilin mouse monoclonal (ab110329, 1:500) were from AbCam. Anti-MICU1 rabbit polyclonal (HPA037480, 1:400) and anti-MCU rabbit polyclonal were from Sigma-Aldrich (HPA016480, WB 1:400, IF 1:100) or from Cell Signaling Technologies (CST D2Z3B, WB 1:500, IF 1:100). Anti-HSP70 mouse monoclonal (MA3–028, WB 1:500, IF 1:50) and anti-RyR2 mouse monoclonal (MA3–916, WB 1:500, IF 1:50) were from Thermo Scientific. Anti-calnexin rabbit polyclonal (ADI-SPA865, 1:500) was from Enzo Life Sciences. Anti-EMRE rabbit polyclonal (sc86337, 1:200) was from Santa Cruz Biotechnology, Inc., and Tim 23 Mouse Monoclonal (611222, 1:500) was from BD Biosciences. Secondary antibodies for IF were as follows. AF 647 (A21244, 1:200) and Alexa Fluor®488 (A21200, 1:200) were from Thermo Fisher, Cy3B (715165150, 1:200) was from Jackson Immunoresearch, and CF™568 (20105, 1:200) was from Biotium. Cell culture medium reagents were obtained from Gibco.

Animals—All of the studies were done in accordance with the National Institutes of Health Guide for the Care and Use of Laboratory Animals, and the protocols were applied in compliance with the Thomas Jefferson University institutional review board guidelines. Male Sprague-Dawley rats of 300–350 g and C57BL/6 mice of 25–30 g body weight were used to obtain heart homogenates and to isolate adult cardiomyocytes. MCUKO mice were housed/maintained in NIH-NHLBI 1 and used in the Murphy (cardiomyocyte isolation) and Finkel (heart homogenates and membrane fractions) laboratories. The cardiac muscle-specific Mfn2KO (Mfn2 flox/flox, MYH6 Cre) mouse colony originated from Gerald Dorn (Washington University, St. Louis, MO) and was maintained as described (44).

Primary Mouse Cardiomyocyte Isolation and Fixation—Mice were anesthetized and anticoagulated using a subcutaneous pentobarbital (90 mg/kg) and heparin (50 IU/mice) injection. The heart was removed and mounted on a Langendorff system, and the cardiomyocyte isolation was done according to the protocol of O'Connell *et al.* (47). The isolated cardiomyocytes were plated onto 25-mm coverglasses freshly precoated with laminin (10 μg/ml) in an extracellular "plating" buffer composed of minimum Eagle's medium + GlutaMAX™ (Gibco) supplemented with BSA (0.1%), penicillin (100 units/ml), BDM (10 mM), insulin (5 μg/ml)/transferrin (5 μg/ml)/selenium (5 ng/ml) (Sigma-Aldrich, catalog no. I-1884) and left to attach for at least 1 h inside the incubator (37 °C and 2% of CO_2). For super-resolution imaging, the cells were plated to laminin-coated glass-bottom dishes (35-mm Petri dish with 10-mm well and No. 1.5 glass from MatTek). After attachment, the cardiomyocytes were loaded (or not) with 50 nM MtTrRed (10–15 min at 37 °C) and then fixed in 40 g/liter paraformaldehyde in PBS (15 min, 20–23 °C), washed with PBS, and kept in PBS at 4 °C until the immunofluorescence procedure.

Heart Mitochondria and SR Isolation—After excising the heart, all steps were done on ice, and centrifuge steps were done at 4 °C. Mice were euthanized by cervical dislocation, and the heart was immediately excised, washed, and placed in isolation buffer, containing 225 mM mannitol, 75 mM sucrose, 20 mM HEPES, 0.1 mM EGTA, and 1 g/liter BSA, pH 7.4. Ventricular muscle tissue was carefully minced, rinsed, and then homogenized with a 5-ml glass-Teflon homogenizer (Wheaton) (~20 up-down strokes at 300 rpm). Crude mitochondrial and SR fractions and rat cardiac muscle homogenates were prepared as described earlier (24) with minor modifications as follows. The homogenate was centrifuged at 500 × *g* for 10 min, and the supernatant was filtered through a 100-μm mesh nylon sieve and further centrifuged at 9,000 × *g* for 10 min. The pellet corresponding to the crude heart mitochondrial fraction (mitochondrial fraction from here on) was resuspended in storage buffer (225 mM mannitol, 75 mM sucrose, and 10 mM HEPES, pH 7.4). The supernatant was centrifuged at 40,000 × *g* for 45 min, and the pellet corresponding to the crude heart jSR (referred to as the SR fraction throughout) was also resuspended in storage buffer. Percoll purification of the mitochondrial fraction was done as described previously (24). Rats were euthanized by decapitation. The heart was immediately removed, and mitochondrial and SR fractions were prepared as described earlier (24), except that the mitochondrial fraction was sedimented at 8,500 × *g*, and the same storage buffer was used for both the mitochondrial and SR fractions.

Skeletal Muscle Mitochondria and SR Isolation—Rats were euthanized as described above, and skeletal muscle was collected right after removal of the heart. All of the following procedures were done on ice. Tibialis anterior and extensor digitorum longus muscles were rapidly excised and placed in Basic Medium containing 140 mM KCl, 20 mM HEPES, 5 mM $MgCl_2$, 2 mM EGTA, pH 7.0. Muscle was cleaned of connective tissue and fat, minced, and transferred into "Homogenizing Medium," which was Basic Medium supplemented with 1 mM ATP and 1% BSA (w/v) and one unit of subtilisin A per g of muscle weight. Tissue was homogenized using a glass/Teflon Potter-Elvehjem homogenizer (500 rpm). Nuclei and unbroken tissue were pelleted at 500 × *g* (10 min). The supernatant was collected and spun at 9,500 × *g* (8 min). The pellet was resuspended in 25 ml of Basic Medium and incubated on ice for 7 min (myofibrillar repolymerization). Samples were spun at 500 × *g* (8 min) to pellet actin-myosin polymers. The supernatant was then spun at 9,500 × *g* (9 min), and the final pellet was resuspended in 500 μl of Basic Medium. To obtain the SR frac-

tion, the supernatant from the first 9,500 × *g* centrifuge step was collected and centrifuged again at 40,000 × *g* (45 min). This pellet was resuspended in 200 μl of Basic Medium.

Protein Analysis and WB—A biuret-based reagent kit from Bio-Rad (DC protein assay kit) was used to measure the protein concentrations for the isolated mitochondria and SR. WB was done using a Bio-Rad setup, including a Trans-Blot® Turbo transfer system. Equal amounts of total protein were loaded (unless otherwise noted), separated electrophoretically by SDS-PAGE (12–15% gels), and transferred to a nitrocellulose membrane. After a blocking step in LI-COR Odyssey blocking solution (1 h at room temperature), the membrane was incubated overnight at 4 °C with primary antibodies. The LI-COR infrared fluorescent secondary antibodies (IRDye 800CW) were used for visualization by means of a LI-COR Odyssey scanner. Band quantification ("densitometry") was performed using ImageJ software (National Institutes of Health).

Isolation of Submitochondrial Membrane Fractions from Rat Heart—Isolation of submitochondrial membrane fractions was performed as described before (22) with slight modification in the sonication parameters for better IMM yield. Briefly, Percoll-purified "heavy" mitochondria were resuspended and incubated in a hyposmotic phosphate buffer ("swelling" buffer: 10 mM NaH_2PO_4/Na_2HPO_4, pH 7.4) for 20 min. Then a "shrinking buffer" (60% sucrose in 29% of final volume) was added. In turn, mitochondrial membranes were disrupted by sonication (Branson 102C CE converter, 3 × 30 s of irradiation at 22% amplitude, 1-min interval), centrifuged at 6,500 × *g* for 10 min. The supernatant was loaded on top of a 30–60% sucrose gradient (see Fig. 1*A*) and spun at 200,000 × *g* for 13 h). Fractions of 1 ml were collected. All procedures were done on ice, and centrifuge steps were at 4 °C.

Enzyme Assays—Monoamine oxidase (MAO) and succinate dehydrogenase (SDH) activity assays were performed and analyzed as described previously (22) except that all enzymatic reactions were measured in a hybrid microplate reader (Biotek Synergy 4). To evaluate citrate synthase activity and IMM intactness, mitochondrial or SR fractions were pretreated with 0.1% Triton X-100 and diluted in Tris-HCl buffer (0.1 M, pH 8) supplemented with 0.1 mM 5,5′-dithiobis(2-nitrobenzoic acid), 0.3 mM acetyl-CoA, and 0.5 mM oxaloacetic acid. Absorbance at 405 nm was tracked for 5 min (10-s intervals). Enzyme activity was expressed as citrate synthase activity units per mg of mitochondrial protein (28). The mitochondrial inner membrane intactness was calculated as the ratio between the citrate synthase activity of the mitochondria preparation in Tris-HCl buffer (0.1 M, pH 8) *versus* the activity of the same mitochondria preparation treated with 0.1% Triton X-100 lysis buffer (giving the percentage of "leaky" or broken mitochondria).

IF of Cells and Isolated Mitochondria—Membrane organelles from the mitochondrial or SR fraction were glued with Cell-Tak™ to coverglasses and loaded with MitoTracker®Red CMXRos (MtTrRed; 50 nM) during attachment (20 min, 20–23 °C) and then fixed (40 g/liter paraformaldehyde/PBS, 10 min). Intracellular medium (120 mM KCl, 10 mM NaCl, 1 mM KH_2PO_4, 20 mM HEPES/Tris, 2 mM NaATP, 2 mM $MgCl_2$) was used for attaching the mitochondria. Fixed mitochondria and cardiomyocytes were subjected to a standard IF staining protocol. 5% goat serum and 0.2% Triton X-100 in PBS were used for blocking and permeabilization. SlowFade® was used for mounting on microscope slides. Secondary antibodies were conjugated with Alexa Fluor®488 or 647 (to minimize spectral overlap with MtTrRed that is excited at 568 nm). To assess nonspecific binding of secondary antibodies, negative controls without primary antibody were used. Specificity of the anti-MCU primary antibodies was tested in knock-out samples as described under "Results" (Figs. 3*A* and 4*A*). Immunofluorescence was imaged using either a Zeiss LSM780MP or LSM510MP confocal microscopes or the LSM880MP system equipped with the Airyscan super-resolution (×1.7 beyond the diffraction limit) detection system. A ×63 Zeiss plan-apochromat oil, 1.4 numerical aperture, differential interference contrast lens was used to obtain all images. Image and colocalization analyses were done using FIJI/ImageJ (National Institutes of Health). After subtracting background using a fluorescence threshold mask, the resulting particles with >0.05-μm^2 area were used. The threshold varied between antibodies, but for each antibody, it was the same. Particle count and areas were determined. Next, overlaps of >0.015 μm^2 between different fluorophores were counted, and their area was measured. Colocalizing particles per all particles and the overlapping area per total area were calculated (for each antibody). For the Airyscan images, the same threshold was applied, but then the RyR2 signal was dilated by 66 nm (1 pixel) from the original labeling. Using this new mask, the same colocalization criterion between MCU and RyR2 was applied. 5–10 microscope fields of 1275 μm^2 were analyzed for each condition.

3D Super-resolution Imaging—3D super-resolution imaging was done using a Vutara 350 microscope equipped with a biplane module, a Hamamatsu ORCA Flash version 4.0 V2 sCMOS camera, and an Olympus Super-Apochromat ×60 water objective with numerical aperture 1.2. Two-color channels were detected sequentially at 50 frames/s (20-ms acquisition time). Laser powers (647- and 561-nm wavelength) were adjusted to provide sufficient fluorophore switching for localization and to minimize photobleaching. Secondary antibodies were conjugated with either Alexa Fluor®647, CF™ 568, or Cy®3b fluorophores. The IF labeling was performed as described above for cells except that the cells were not mounted but kept at 4 °C in PBS until just before the imaging experiments were done. Imaging was performed in an oxidizing buffer containing 10% (w/v) glucose in 10 mM PBS-Tris, pH 7.5, with 10 mM mercaptoethylamine combined with 50 mM β-mercaptoethanol, 2 mM cyclooctatetraene that promoted the reversible photoswitching of the fluorophores conjugated with the secondary antibodies. Data analysis was performed using the Vutara SRX software (version 5.22). Single molecules were identified by their brightness frame by frame after removing the background. Identified particles were then localized in three dimensions by fitting the raw data in a customizable region of interest (typically 16 × 16 pixels) centered on each particle in each plane with a 3D model function that was obtained from recorded bead data sets. Fit results were stored as data lists for further analysis. The image resolution capable of experimentally being achieved is 20 nm laterally (*x* and *y*) and

50 nm axially (in *z*). The nearest neighbor particle analysis was done automatically by the Vutura SRX software. Peripheral *versus* internal localization MCU immunolabeling over the 3D cloud of mtHsP70 (matrix) immunolabeling was established based on *xyz* rotations of individual mitochondria. The positioning of anti-MCU-positive particles in relation to the surface of the mtHsp70-filled volume was determined for 24 randomly selected mitochondria from two different low magnification fields. The software allowed 3D trimming, so information from neighboring mitochondria did not interfere with the rotation views.

Electrical Field Stimulation on Isolated Adult Cardiomyocytes—Electrical field stimulation was performed as described before (48). Briefly, isolated calcium-tolerant cardiomyocytes from adult mouse hearts were placed in 25-mm diameter coverslips pretreated with laminin and mounted in an electrical stimulation chamber equipped with two Pt electrodes (RC-47FSLP, Warner Instruments). Cells were continuously perfused with field stimulation buffer, containing 150 mM NaCl, 5.4 mM KCl, 10 mM HEPES acid, 1 mM glucose, 2 mM pyruvate, 5 mM creatine, and 5 mM taurin, supplemented with 2 μM or 1 mM $CaCl_2$ and BDM (10 mM) to prevent contractions. Electrical biphasic pulses of 20-mV amplitude, 2-Hz frequency, and 5-ms duration were applied to the cells for 10 min (MyoPacer Stimulator, IonOptix).

To record cytosolic Ca^{2+} transients during field stimulation, cardiomyocytes were loaded with 5 μM fura-2 acetoxymethyl ester dissolved into the plating buffer in the presence of 0.003% Pluronic® F127 (Sigma-Aldrich P-2443) for 20 min at room temperature, washed, and briefly postincubated to allow hydrolysis of the acetoxymethyl ester within the cells. Imaging was performed using an Olympus IX81 inverted microscope (Fluo/340 ×40 oil immersion objective, numerical aperture 1.35) fitted with a Lambda DG-4 ultra-high speed wavelength-switch illuminator (Sutter Instruments) and a 512 × 512 EMCCD camera (ImagEM, Hamamatsu, Japan). 340/30-nm and 380/20-nm band pass excitation filters, beam splitter 59022Bs, and dual dichroic 59022M were from Chroma Technologies. Cells were excited alternately with 340-nm and 380-nm wavelengths, and changes in the >500-nm emission were captured. Recordings from each cell were obtained at a rate of 45 ms/frame, and changes in the average ratio (340 nm/380 nm) for previously defined regions of interest were analyzed throughout the stimulation period (Metamorph version 7.8.6.0, Molecular Devices, LLC). Next, cardiomyocytes were fixed and subjected to a standard IF staining protocol and imaged/analyzed as described above for the Zeiss LSM880 Airyscan system.

$^{45}Ca^{2+}$ Retention Assays—Mitochondrial or SR fractions (250 μg/ml) were rapidly resuspended in 350 μl of intracellular medium (120 mM KCl, 10 mM NaCl, 1 mM KH_2PO_4, 20 mM HEPES/Tris, 2 mM NaATP, 2 mM $MgCl_2$) supplemented with protease inhibitors (leupeptin, antipain, and pepstatin; 1 μg/ml each), thapsigargin (Tg; 2 μM), caffeine (10 mM), EGTA/Tris (pH 7.4) (50 μM), and malate and pyruvate (1 mM concentration of each to energize mitochondria). Na^+-dependent mitochondrial Ca^{2+} extrusion and the permeability transition pore were blocked by CGP-37157 (20 μM) and cyclosporine A (2 μM), respectively. After a 20-s incubation at 37 °C, the suspension was transferred to an Eppendorf tube containing a $CaCl_2$ bolus with 8 μCi of $^{45}Ca^{2+}$ to elevate $[Ca^{2+}]_o$ to 0.3 or 1.5 μM. $CaCl_2$ boluses were pretitrated in fluorometric assays (see below). After a 15-s, 30-s, and 4-min incubation at 37 °C, 100-μl aliquots were rapidly diluted in 5 ml of ice-cold washing buffer (140 mM KCl, 10 mM Hepes/Tris, 0.5 mM EGTA/Tris, pH 7.2) and filtered through 0.3-μm nitrocellulose filters (Millipore). Filters were rinsed once with washing buffer, and $^{45}Ca^{2+}$ in the captured membrane particles was quantified by liquid scintillation counting.

Fluorometric Measurements of $[Ca^{2+}]_o$—Mitochondrial or SR fractions were resuspended in 1.5 ml of intracellular medium supplemented with Tg, caffeine, protease inhibitors, malate/pyruvate, and (for $[Ca^{2+}]_o$ measurements) EGTA/Tris (50 μM), in a stirred thermostated (37 °C) cuvette inside a multiwavelength excitation and dual-emission fluorometer (DeltaRAM, PTI). $[Ca^{2+}]_o$ was measured using fura2 (1.5 μM) for $[Ca^{2+}]_o$ range 0 to ~2.5 μM or fura-loAff (1 μM) for $[Ca^{2+}]_o$ >2.5 μM. Fura fluorescence was recorded and transformed to molar $[Ca^{2+}]$ values as described (36). Despite the Ca^{2+}-free isolation procedure at 0–4 °C, significant Ca^{2+} residue remained in the SR store of the SR fraction. This was discharged by the Tg and caffeine without increasing the (EGTA-stabilized) baseline (which remained <40 nM) but decreasing the $CaCl_2$ bolus that was needed to reach the target $[Ca^{2+}]_o$.

Gel Filtration (Size Exclusion) Chromatography—Rat mitochondrial and SR fractions were solubilized in an ice-cold buffer containing 3% CHAPS, 120 mM KCl, 20 mM MOPS, and 0.5 mM EDTA for 5 min. Then the resulting sample was centrifuged at 40,000 rpm (~57,000 × *g*) at 4 °C. The supernatant was loaded on top of a Sephacryl-S400 HR chromatography column (GE Healthcare, 17-0609-05). The column was equilibrated in 120 mM KCl, 20 mM MOPS, 0.5 mM EDTA, and 0.75% CHAPS. 24 0.5-ml fractions were collected, and 25 μl of each were analyzed by WB. WB profiles were determined from equal volumes of the fractions because there was no significant difference in their protein content over the relevant range (fractions 9–22; Fig. 10*A*)

TEM—Rat heart was fixed and processed for TEM as described earlier (22). High pressure freezing and freeze-substitution were carried out in the University of Pennsylvania Electron Microscopy Resource Laboratory. Samples (mitochondrial and SR fraction suspension droplets from one rat heart) were frozen vitreously in an Abra HPM010 machine and dehydrated at −100 °C in 100% acetone, 2% OsO_4, 0.1% uranyl acetate for 48 h. Samples were warmed to room temperature, washed in acetone, and embedded in EPON resin before polymerization. Material containing sample was sectioned at 60-nm thickness, mounted on TEM grids, and secondarily stained with 2% aqueous uranyl acetate and Reynold's lead citrate before observation at 80 keV on a JEOL JEM1010 or FEI Tecnai 12 transmission election microscope. Images were digitally collected on a Hamamatsu CCD camera with AMT software. Organelle and membrane particle metrics were taken by FIJI/ImageJ. Mitochondria with no major disruption in the OMM line and recognizable IMM/cristae were considered "well defined."

Statistical Analysis—Data are presented as mean ± S.E. Experiments were performed at least three times unless otherwise noted. Statistical analysis was performed using Student's *t* test or the Mann-Whitney rank sum test. Single and double asterisks in the graphs indicate $p \leq 0.05$ and $p \leq 0.01$, respectively.

Author Contributions—S. D. L. F. performed most of the experiments, analyzed data, and critically read and wrote parts of the manuscript. C. V. did some of the experiments for MCU distribution in submitochondrial fractions and analyzed the data. C. F.-S. carried out the citrate synthase assays, field stimulation, and Ca^{2+} imaging in the adult cardiomyocytes, analyzed data, read the manuscript, and wrote the relevant part under "Experimental Procedures." E. J. A. did the IF studies in control *versus* MCUKD HeLa cells. K. H. and J. S. assisted with the cardiomyocyte and mitochondria isolation from the MCU KO mice at NHLBI, National Institutes of Health, under the supervision of T. F. and E. M., and all critically read the manuscript. J. M. performed some of the Western blotting. D. W. performed the high pressure freezing and freeze-substitution. S. K. J. led/supervised the gel filtration chromatography assays and their analysis, supervised the $45Ca^{2+}$ assays, and critically read the manuscript. S.-S. S. designed experiments and critically read/edited the manuscript. G. C. conceived the project, designed experiments, performed TEM imaging and analysis, and wrote the manuscript.

Acknowledgments—We are grateful to Ludovic Gomez for training S. F. for mouse cardiomyocyte isolation. We thank Gyorgy Hajnoczky for all of the invaluable discussions and critical reading of the manuscript. We also thank Gudheti Manasa for vital assistance in using the Vutara super-resolution microscopy demo system. We thank David Weaver (MitoCare) for further help with the super-resolution imaging.

References

1. Bernardi, P. (1999) Mitochondrial transport of cations: channels, exchangers, and permeability transition. *Physiol. Rev.* **79,** 1127–1155
2. Kirichok, Y., Krapivinsky, G., and Clapham, D. E. (2004) The mitochondrial calcium uniporter is a highly selective ion channel. *Nature* **427,** 360–364
3. Sancak, Y., Markhard, A. L., Kitami, T., Kovács-Bogdan, E., Kamer, K. J., Udeshi, N. D., Carr, S. A., Chaudhuri, D., Clapham, D. E., Li, A. A., Calvo, S. E., Goldberger, O., and Mootha, V. K. (2013) EMRE is an essential component of the mitochondrial calcium uniporter complex. *Science* **342,** 1379–1382
4. Kovács-Bogdán, E., Sancak, Y., Kamer, K. J., Plovanich, M., Jambhekar, A., Huber, R. J., Myre, M. A., Blower, M. D., and Mootha, V. K. (2014) Reconstitution of the mitochondrial calcium uniporter in yeast. *Proc. Natl. Acad. Sci. U.S.A.* **111,** 8985–8990
5. Tsai, M. F., Phillips, C. B., Ranaghan, M., Tsai, C. W., Wu, Y., Willliams, C., and Miller, C. (2016) Dual functions of a small regulatory subunit in the mitochondrial calcium uniporter complex. *eLife* **5,** e15545
6. Vais, H., Mallilankaraman, K., Mak, D. O., Hoff, H., Payne, R., Tanis, J. E., and Foskett, J. K. (2016) EMRE is a matrix Ca^{2+} sensor that governs gatekeeping of the mitochondrial Ca^{2+} uniporter. *Cell Rep.* **14,** 403–410
7. Yamamoto, T., Yamagoshi, R., Harada, K., Kawano, M., Minami, N., Ido, Y., Kuwahara, K., Fujita, A., Ozono, M., Watanabe, A., Yamada, A., Terada, H., and Shinohara, Y. (2016) Analysis of the structure and function of EMRE in a yeast expression system. *Biochim. Biophys. Acta* **1857,** 831–839
8. Mammucari, C., Raffaello, A., Vecellio Reane, D., and Rizzuto, R. (2016) Molecular structure and pathophysiological roles of the Mitochondrial Calcium Uniporter. *Biochim. Biophys. Acta* **1863,** 2457–2464
9. Raffaello, A., De Stefani, D., Sabbadin, D., Teardo, E., Merli, G., Picard, A., Checchetto, V., Moro, S., Szabò, I., and Rizzuto, R. (2013) The mitochondrial calcium uniporter is a multimer that can include a dominant-negative pore-forming subunit. *EMBO J.* **32,** 2362–2376
10. Spät, A., Szanda, G., Csordás, G., and Hajnóczky, G. (2008) High- and low-calcium-dependent mechanisms of mitochondrial calcium signalling. *Cell Calcium* **44,** 51–63
11. Balaban, R. S. (2002) Cardiac energy metabolism homeostasis: role of cytosolic calcium. *J. Mol. Cell. Cardiol.* **34,** 1259–1271
12. Csordás, G., Thomas, A. P., and Hajnóczky, G. (2001) Calcium signal transmission between ryanodine receptors and mitochondria in cardiac muscle. *Trends Cardiovasc. Med.* **11,** 269–275
13. Sharma, V. K., Ramesh, V., Franzini-Armstrong, C., and Sheu, S. S. (2000) Transport of Ca^{2+} from sarcoplasmic reticulum to mitochondria in rat ventricular myocytes. *J. Bioenerg. Biomembr.* **32,** 97–104
14. Chacon, E., Ohata, H., Harper, I. S., Trollinger, D. R., Herman, B., and Lemasters, J. J. (1996) Mitochondrial free calcium transients during excitation-contraction coupling in rabbit cardiac myocytes. *FEBS Lett.* **382,** 31–36
15. Boyman, L., Chikando, A. C., Williams, G. S., Khairallah, R. J., Kettlewell, S., Ward, C. W., Smith, G. L., Kao, J. P., and Lederer, W. J. (2014) Calcium movement in cardiac mitochondria. *Biophys. J.* **107,** 1289–1301
16. Holmström, K. M., Pan, X., Liu, J. C., Menazza, S., Liu, J., Nguyen, T. T., Pan, H., Parks, R. J., Anderson, S., Noguchi, A., Springer, D., Murphy, E., and Finkel, T. (2015) Assessment of cardiac function in mice lacking the mitochondrial calcium uniporter. *J. Mol. Cell. Cardiol.* **85,** 178–182
17. Pan, X., Liu, J., Nguyen, T., Liu, C., Sun, J., Teng, Y., Fergusson, M. M., Rovira, I. I., Allen, M., Springer, D. A., Aponte, A. M., Gucek, M., Balaban, R. S., Murphy, E., and Finkel, T. (2013) The physiological role of mitochondrial calcium revealed by mice lacking the mitochondrial calcium uniporter. *Nat. Cell Biol.* **15,** 1464–1472
18. Kwong, J. Q., Lu, X., Correll, R. N., Schwanekamp, J. A., Vagnozzi, R. J., Sargent, M. A., York, A. J., Zhang, J., Bers, D. M., and Molkentin, J. D. (2015) The mitochondrial calcium uniporter selectively matches metabolic output to acute contractile stress in the heart. *Cell Rep.* **12,** 15–22
19. Luongo, T. S., Lambert, J. P., Yuan, A., Zhang, X., Gross, P., Song, J., Shanmughapriya, S., Gao, E., Jain, M., Houser, S. R., Koch, W. J., Cheung, J. Y., Madesh, M., and Elrod, J. W. (2015) The mitochondrial calcium uniporter matches energetic supply with cardiac workload during stress and modulates permeability transition. *Cell Rep.* **12,** 23–34
20. Rasmussen, T. P., Wu, Y., Joiner, M. L., Koval, O. M., Wilson, N. R., Luczak, E. D., Wang, Q., Chen, B., Gao, Z., Zhu, Z., Wagner, B. A., Soto, J., McCormick, M. L., Kutschke, W., Weiss, R. M., *et al.* (2015) Inhibition of MCU forces extramitochondrial adaptations governing physiological and pathological stress responses in heart. *Proc. Natl. Acad. Sci. U.S.A.* **112,** 9129–9134
21. Fieni, F., Lee, S. B., Jan, Y. N., and Kirichok, Y. (2012) Activity of the mitochondrial calcium uniporter varies greatly between tissues. *Nat. Commun.* **3,** 1317
22. García-Pérez, C., Schneider, T. G., Hajnóczky, G., and Csordás, G. (2011) Alignment of sarcoplasmic reticulum-mitochondrial junctions with mitochondrial contact points. *Am. J. Physiol. Heart Circ. Physiol.* **301,** H1907–H1915
23. Kamer, K. J., and Mootha, V. K. (2015) The molecular era of the mitochondrial calcium uniporter. *Nat. Rev. Mol. Cell Biol.* **16,** 545–553
24. García-Pérez, C., Hajnóczky, G., and Csordás, G. (2008) Physical coupling supports the local Ca^{2+} transfer between sarcoplasmic reticulum subdomains and the mitochondria in heart muscle. *J. Biol. Chem.* **283,** 32771–32780
25. Antony, A. N., Paillard, M., Moffat, C., Juskeviciute, E., Correnti, J., Bolon, B., Rubin, E., Csordás, G., Seifert, E. L., Hoek, J. B., and Hajnóczky, G. (2016) MICU1 regulation of mitochondrial Ca^{2+} uptake dictates survival and tissue regeneration. *Nat. Commun.* **7,** 10955
26. Wieckowski, M. R., Giorgi, C., Lebiedzinska, M., Duszynski, J., and Pinton, P. (2009) Isolation of mitochondria-associated membranes and mitochondria from animal tissues and cells. *Nat. Protoc.* **4,** 1582–1590
27. Franzini-Armstrong, C. (2007) ER-mitochondria communication: how privileged? *Physiology* **22,** 261–268

28. Boengler, K., Ruiz-Meana, M., Gent, S., Ungefug, E., Soetkamp, D., Miro-Casas, E., Cabestrero, A., Fernandez-Sanz, C., Semenzato, M., Di Lisa, F., Rohrbach, S., Garcia-Dorado, D., Heusch, G., and Schulz, R. (2012) Mitochondrial connexin 43 impacts on respiratory complex I activity and mitochondrial oxygen consumption. *J. Cell. Mol. Med.* **16,** 1649–1655
29. Despa, S., Shui, B., Bossuyt, J., Lang, D., Kotlikoff, M. I., and Bers, D. M. (2014) Junctional cleft $[Ca^{2+}]_i$ measurements using novel cleft-targeted Ca^{2+} sensors. *Circ. Res.* **115,** 339–347
30. Kushnareva, Y. E., Gerencser, A. A., Bossy, B., Ju, W. K., White, A. D., Waggoner, J., Ellisman, M. H., Perkins, G., and Bossy-Wetzel, E. (2013) Loss of OPA1 disturbs cellular calcium homeostasis and sensitizes for excitotoxicity. *Cell Death Differ.* **20,** 353–365
31. Fülöp, L., Szanda, G., Enyedi, B., Várnai, P., and Spät, A. (2011) The effect of OPA1 on mitochondrial Ca^{2+} signaling. *PLoS One* **6,** e25199
32. Lu, X., Ginsburg, K. S., Kettlewell, S., Bossuyt, J., Smith, G. L., and Bers, D. M. (2013) Measuring local gradients of intramitochondrial $[Ca^{2+}]$ in cardiac myocytes during sarcoplasmic reticulum Ca^{2+} release. *Circ. Res.* **112,** 424–431
33. Baughman, J. M., Perocchi, F., Girgis, H. S., Plovanich, M., Belcher-Timme, C. A., Sancak, Y., Bao, X. R., Strittmatter, L., Goldberger, O., Bogorad, R. L., Koteliansky, V., and Mootha, V. K. (2011) Integrative genomics identifies MCU as an essential component of the mitochondrial calcium uniporter. *Nature* **476,** 341–345
34. Patron, M., Checchetto, V., Raffaello, A., Teardo, E., Vecellio Reane, D., Mantoan, M., Granatiero, V., Szabò, I., De Stefani, D., and Rizzuto, R. (2014) MICU1 and MICU2 finely tune the mitochondrial Ca^{2+} uniporter by exerting opposite effects on MCU activity. *Mol. Cell* **53,** 726–737
35. Oxenoid, K., Dong, Y., Cao, C., Cui, T., Sancak, Y., Markhard, A. L., Grabarek, Z., Kong, L., Liu, Z., Ouyang, B., Cong, Y., Mootha, V. K., and Chou, J. J. (2016) Architecture of the mitochondrial calcium uniporter. *Nature* **533,** 269–273
36. Csordás, G., Golenár, T., Seifert, E. L., Kamer, K. J., Sancak, Y., Perocchi, F., Moffat, C., Weaver, D., de la Fuente Perez, S., Bogorad, R., Koteliansky, V., Adijanto, J., Mootha, V. K., and Hajnóczky, G. (2013) MICU1 controls both the threshold and cooperative activation of the mitochondrial Ca^{2+} uniporter. *Cell Metab.* **17,** 976–987
37. Mallilankaraman, K., Doonan, P., Cárdenas, C., Chandramoorthy, H. C., Müller, M., Miller, R., Hoffman, N. E., Gandhirajan, R. K., Molgó, J., Birnbaum, M. J., Rothberg, B. S., Mak, D. O., Foskett, J. K., and Madesh, M. (2012) MICU1 is an essential gatekeeper for MCU-mediated mitochondrial Ca^{2+} uptake that regulates cell survival. *Cell* **151,** 630–644
38. Liu, J. C., Liu, J., Holmström, K. M., Menazza, S., Parks, R. J., Fergusson, M. M., Yu, Z. X., Springer, D. A., Halsey, C., Liu, C., Murphy, E., and Finkel, T. (2016) MICU1 serves as a molecular gatekeeper to prevent *in vivo* mitochondrial calcium overload. *Cell Rep.* **16,** 1561–1573
39. Huang, X., Sun, L., Ji, S., Zhao, T., Zhang, W., Xu, J., Zhang, J., Wang, Y., Wang, X., Franzini-Armstrong, C., Zheng, M., and Cheng, H. (2013) Kissing and nanotunneling mediate intermitochondrial communication in the heart. *Proc. Natl. Acad. Sci. U.S.A.* **110,** 2846–2851
40. Parfenov, A. S., Salnikov, V., Lederer, W. J., and Lukyánenko, V. (2006) Aqueous diffusion pathways as a part of the ventricular cell ultrastructure. *Biophys. J.* **90,** 1107–1119
41. de Brito, O. M., and Scorrano, L. (2008) Mitofusin 2 tethers endoplasmic reticulum to mitochondria. *Nature* **456,** 605–610
42. Filadi, R., Greotti, E., Turacchio, G., Luini, A., Pozzan, T., and Pizzo, P. (2015) Mitofusin 2 ablation increases endoplasmic reticulum-mitochondria coupling. *Proc. Natl. Acad. Sci. U.S.A.* **112,** E2174–E2181
43. Cosson, P., Marchetti, A., Ravazzola, M., and Orci, L. (2012) Mitofusin-2 independent juxtaposition of endoplasmic reticulum and mitochondria: an ultrastructural study. *PLoS One* **7,** e46293
44. Chen, Y., Csordás, G., Jowdy, C., Schneider, T. G., Csordás, N., Wang, W., Liu, Y., Kohlhaas, M., Meiser, M., Bergem, S., Nerbonne, J. M., Dorn, G. W., 2nd, and Maack, C. (2012) Mitofusin 2-containing mitochondrial-reticular microdomains direct rapid cardiomyocyte bioenergetic responses via interorganelle Ca^{2+} crosstalk. *Circ. Res.* **111,** 863–875
45. Neupert, W. (1997) Protein import into mitochondria. *Annu. Rev. Biochem.* **66,** 863–917
46. Boncompagni, S., Rossi, A. E., Micaroni, M., Beznoussenko, G. V., Polishchuk, R. S., Dirksen, R. T., and Protasi, F. (2009) Mitochondria are linked to calcium stores in striated muscle by developmentally regulated tethering structures. *Mol. Biol. Cell* **20,** 1058–1067
47. O'Connell, T. D., Rodrigo, M. C., and Simpson, P. C. (2007) Isolation and culture of adult mouse cardiac myocytes. *Methods Mol. Biol.* **357,** 271–296
48. Fernandez-Sanz, C., Ruiz-Meana, M., Miro-Casas, E., Nuñez, E., Castellano, J., Loureiro, M., Barba, I., Poncelas, M., Rodriguez-Sinovas, A., Vázquez, J., and Garcia-Dorado, D. (2014) Defective sarcoplasmic reticulum-mitochondria calcium exchange in aged mouse myocardium. *Cell Death Dis.* **5,** e1573